Cell

Eukaryotic Stress Granules Are Cleared by Autophagy and Cdc48/VCP Function

J. Ross Buchan,[1,3] Regina-Maria Kolaitis,[2,3] J. Paul Taylor,[2,*] and Roy Parker[1,*]
[1]Department of Chemistry and Biochemistry and Howard Hughes Medical Institute, University of Colorado Boulder, Boulder, CO 80303, USA
[2]Department of Developmental Neurobiology, St. Jude Children's Research Hospital, Memphis, TN 38105, USA
[3]These authors contributed equally to this work
*Correspondence: jpaul.taylor@stjude.org (J.P.T.), roy.parker@colorado.edu (R.P.)
http://dx.doi.org/10.1016/j.cell.2013.05.037

SUMMARY

Stress granules and P bodies are conserved cytoplasmic aggregates of nontranslating messenger ribonucleoprotein complexes (mRNPs) implicated in the regulation of mRNA translation and decay and are related to RNP granules in embryos, neurons, and pathological inclusions in some degenerative diseases. Using baker's yeast, 125 genes were identified in a genetic screen that affected the dynamics of P bodies and/or stress granules. Analyses of such mutants, including *CDC48* alleles, provide evidence that stress granules can be targeted to the vacuole by autophagy, in a process termed granulophagy. Moreover, stress granule clearance in mammalian cells is reduced by inhibition of autophagy or by depletion or pathogenic mutations in valosin-containing protein (*VCP*), the human ortholog of *CDC48*. Because mutations in *VCP* predispose humans to amyotrophic lateral sclerosis, frontotemporal lobar degeneration, inclusion body myopathy, and multisystem proteinopathy, this work suggests that autophagic clearance of stress granule related and pathogenic RNP granules that arise in degenerative diseases may be important in reducing their pathology.

INTRODUCTION

The control of mRNA translation, localization, and degradation plays an important role in the proper modulation of gene expression. Such posttranscriptional control is emphasized in many biological conditions including stress responses, embryogenesis, and synaptic plasticity (Spriggs et al., 2010; Medioni et al., 2012; Doyle and Kiebler, 2011; Gkogkas et al., 2010). Key issues in understanding posttranscriptional control mechanisms include understanding the messenger ribonucleoprotein complexes (mRNPs) that form and how the cell controls the translation, localization, and degradation of such mRNPs.

In the last decade, it has become clear that nontranslating mRNPs in eukaryotic cells often assemble into conserved and dynamic cytoplasmic mRNP granules known as P bodies and stress granules (Erickson and Lykke-Andersen, 2011; Anderson and Kedersha, 2009; Buchan and Parker, 2009). Stress granules are typically observed when translation initiation is limiting and consist of mRNAs associated with some translation initiation factors and RNA binding proteins, and thus are thought to represent a pool of mRNPs stalled in the process of translation initiation (Anderson and Kedersha, 2009; Buchan and Parker, 2009). P bodies consist of mRNAs associated with translation repressors and the mRNA decay machinery, and, although typically present in cells at modest levels, they increase when the pool of nontranslating mRNPs is larger (Parker and Sheth, 2007).

P bodies and stress granules are of interest because they have been connected to a number of important cellular processes including normal mRNA degradation (Sheth and Parker, 2003), nonsense mediated decay (Sheth and Parker, 2006; Franks et al., 2010), microRNA (miRNA) function (Bhattacharyya et al., 2006; Leung et al., 2006), viral replication (Beckham and Parker 2008), and cell signaling (Arimoto et al., 2008; Takahara and Maeda, 2012). In addition, P bodies and stress granules are related to mRNP granules found in neurons, which are involved in mRNA transport and translational control at synapses, and to mRNP granules in embryogenesis where maternal mRNAs are stored (Anderson and Kedersha, 2009; Buchan and Parker, 2009).

More recently, stress granules have emerged as being involved in some degenerative diseases. For example, conditions such as amyotrophic lateral sclerosis (ALS), frontotemporal lobar degeneration (FTLD), fragile X syndrome, spinocerebellar ataxia-2, inclusion body myopathy (IBM), and multisystem proteinopathy (MSP) can result from mutations in known stress-granule proteins that often increase their tendency to aggregate (Ito and Suzuki, 2011; Didiot et al., 2009; Nonhoff et al., 2007; Kim et al., 2013). Additionally, a hallmark of ALS, FTLD, and some other degenerative diseases is the accumulation of cytoplasmic aggregates that contain several stress granule factors and RNA (Dewey et al., 2012; Ito and Suzuki, 2011; Ginsberg et al., 1998). This leads to the hypothesis that inappropriate formation or persistence of stress granules, or some related mRNP aggregate, might be related to the pathogenesis in these diseases. Interestingly, mutations in valosin-containing protein (VCP) cause ALS, FTLD, and MSP, which are all characterized by pathological accumulation of TDP-43 and in some cases other stress granule proteins in cytoplasmic aggregates

(Johnson et al., 2010; Salajegheh et al., 2009; Kim et al., 2013), raising the possibility that VCP is involved in stress granule dynamics.

The formation of stress granules and P bodies is based on two principles. First, they require nontranslating RNA for their assembly. Second, individual mRNPs are brought together by dimerization or aggregation domains present on mRNP binding proteins. For example, the assembly of P bodies in yeast is driven in part by a dimerization domain on the Edc3 protein and a "prion domain" present on the Lsm4 protein (Decker et al., 2007; Reijns et al., 2008). Similarly, stress granule formation in mammalian cells is promoted by a prion domain on the TIA1 protein (Gilks et al., 2004), and mRNA binding proteins frequently contain such aggregation-prone prion-like or low-complexity domains (Decker et al., 2007; Kato et al., 2012; Kim et al., 2013). The prevalence of such aggregation domains in RNA binding proteins as part of their normal role in forming stress granules and P bodies suggests they provide a significant target for mutations that create pathologically aggregated proteins.

Given the biological roles of stress granules and P bodies, as well as their connection to degenerative diseases, an important goal is to understand the mechanisms that control stress granule and P body assembly, disassembly, and clearance from the cell. To identify proteins involved in modulating these mRNP granules, we performed a genetic screen in *S. cerevisiae* to identify mutations that altered stress granules or P bodies. We examined yeast mutants under normal growth conditions rather than stress, as this allowed us to better distinguish mutations that give constitutive stress granules or elevated P bodies, perhaps due to defects in disassembly or clearance mechanisms. We identified over 100 highly interconnected genes that affect stress granules and/or P bodies. Additional analyses provided evidence that clearance of these mRNP granules is affected by both autophagy and Cdc48/VCP function, thus identifying a new mechanism for clearing these assemblies from the cell, which may also play a role in clearing toxic RNPs from mammalian cells to limit pathologies.

RESULTS

Identification of Proteins Affecting P Body and Stress Granule Assembly

A microscopy-based screen of 4,249 nonessential gene deletions (Table S1 available online) in *S. cerevisiae* was conducted to determine genes whose absence alters P body or stress granule assembly. For this screen, the stress granule component, Pab1-GFP, and the P body component, Edc3-mCh, were introduced into each strain on a centromere plasmid. Each mutant strain was examined microscopically under good growth conditions where P bodies are small, allowing us to detect increases and decreases in P bodies, and stress granules are almost completely absent, allowing us to identify mutants with constitutive stress granules.

We identified 125 mutants that gave reproducible stress granules and/or P body phenotypes (see below). For each mutant, the phenotype was verified by repeat experiments, and the gene deletion was verified by PCR and sequencing analysis. Expression levels of Pab1-GFP in a subset of the screen deletion hits showed only modest variation; thus, the observed phenotypes are generally unlikely to be due to altered granule protein expression levels (Figure S1). Phenotypes varied as to the effect on stress granules and P bodies, and the severity of the phenotype (summarized in Tables S2 and S3; examples in Figure 1A), and included increased stress granules associated with P bodies (81 genes), increased stress granules distinct from P bodies (20 genes), increased P bodies (28 genes), decreased P bodies (23 genes), and intravacuolar accumulation of Pab1 and Edc3 (1 gene). These subcategories total to more than 125 because some mutants have more than one phenotype. In most cases, the observed Pab1-GFP foci contain another stress granule component, Pub1-mCh, indicating they represent stress granules (Figure S2).

The 125 genes identified in our screen exhibited diverse functions according to gene ontology (GO) term analysis (Figure 1B), but network analysis reveals a remarkably interconnected genetic and physical network formed by 100/125 of the screen hits, involving 448 nonredundant connections (Figure 1C; p value of 5.34×10^{-6}, see Experimental Procedures). These interconnections suggest these factors form a previously unknown network regulating mRNP-granule formation.

Several mutants mapped to specific complexes or pathways in yeast cells, typically with similar phenotypes within each grouping (Figure S3A; Table S2). For example, multiple defects in the THO and TREX-2 complexes (*hpr1Δ*, *mft1Δ*, *sac3Δ*, *thp1Δ*, *thp2Δ*, and *tho2Δ*), which function in coupling transcription to mRNA export, showed constitutive stress granules, and in a smaller subset of cells nuclear accumulation of Pab1. Similarly, mutations in three subunits of the prefoldin complex (*gim4Δ*, *pfd1Δ*, *gim5Δ*) gave decreased P bodies (Figure S3A). In a final example, we observed that deletions of five subunits of the vacuolar ATPase complex (*vma11Δ*, *vma16Δ*, *vma2Δ*, *vma4Δ*, and *vma3Δ*), and a chaperone required for its assembly (*vma21Δ*) gave increased stress granules (Figure S3A). The vacuolar ATPase might affect stress granule dynamics by direct contacts to mRNAs because the Vma1 subunit has recently been identified as an mRNP binding protein (Mitchell et al., 2013), and we observe that Vma2 colocalizes with P bodies and stress granules under stress conditions (Figure S3B). Alternatively, the vacuolar ATPase may affect stress granules by altering membrane dynamics, which can affect autophagy (Yamamoto et al., 1998; Mijaljica et al., 2011; see below).

Yeast Stress Granules and P Bodies Can Be Targeted for Autophagy

An important result was that several mutations that disrupt autophagy (*atg8Δ*, *atg11Δ*, *atg18Δ*, *mon1Δ*, and *meh1Δ*) gave an increase in constitutive stress granules, which were typically associated with P bodies (Figure 2A; Table S2). In addition, we observed the accumulation of Pab1-GFP and Edc3-mCh in an intravacuolar compartment (referred to as the IVC) in *atg15Δ* mutants (Figure 2A). Moreover, this IVC seen in the *atg15Δ* strain also contains other components of stress granules including Pbp1, Ded1, and Pub1 (Figure S4). This is consistent with the fact that Atg15 is a vacuolar lipase that helps break open vesicles targeted to the vacuole from autophagic trafficking pathways (Teter et al., 2001). These observations argue that stress

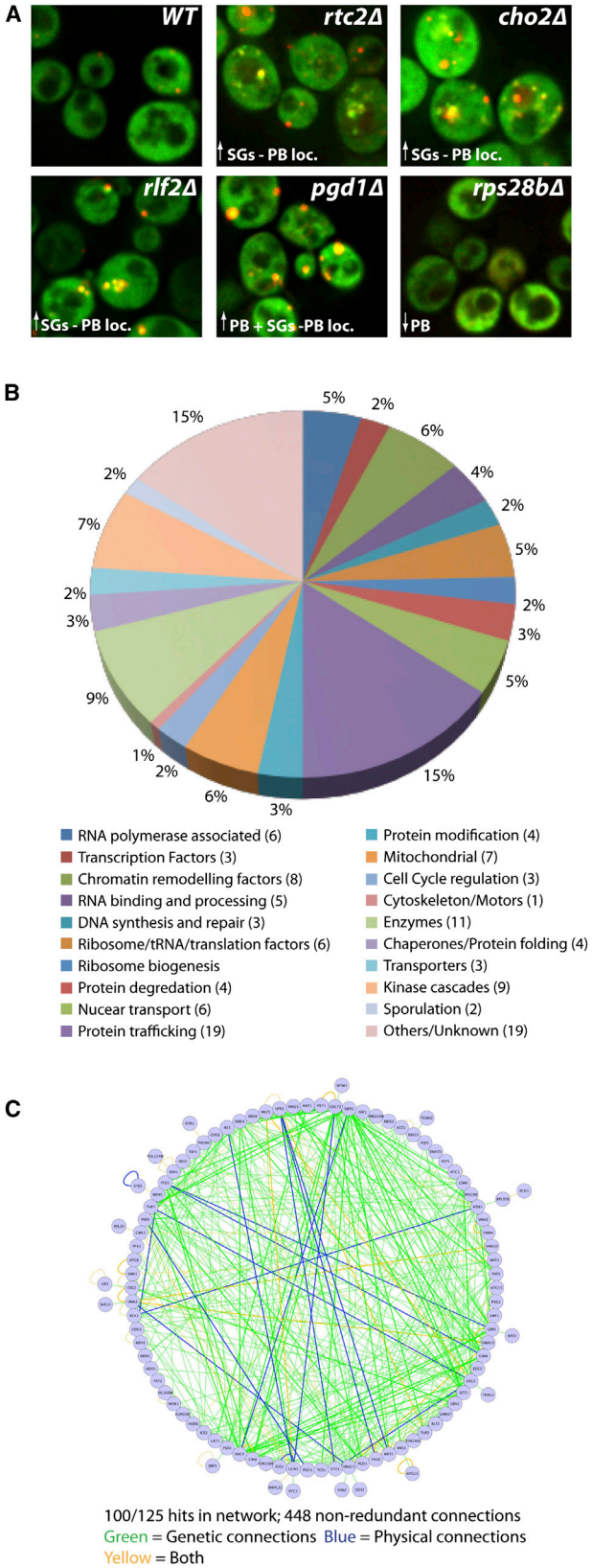

Figure 1. Overview of Screen for Genes Affecting Stress Granule and P Body Assembly

(A) Typical screen phenotypes (log growth). Pab1-GFP and Edc3-mCh serve as stress granule and P body markers respectively. Examples of P body localized stress granules (*rtc2Δ*, *cho2Δ*, *rlf2Δ*), increased P bodies (*pgd1Δ*), and decreased P bodies (*rp28bΔ*) are shown.

(B) One hundred twenty-five screen hits categorized by GO terms.

(C) Network analysis of known physical and genetic connections of screen hits. See also Figures S1, S2, and S3 and Tables S1, S2, S3, S4, and S5.

granules and P bodies can be targeted to the vacuole by autophagy, and therefore, in strains defective in autophagy, stress granules and P bodies accumulate in the cytosol, or within the vacuole when late steps in autophagic vesicle breakdown are defective as in the *atg15Δ* strain.

Consistent with this interpretation, in wild-type cells we observed a small degree of colocalization between both Pub1-mCh or Edc3-mCh foci with Atg11-GFP or Atg19-GFP (Figures S5 and S6; Table S4). Atg11 and Atg19 both facilitate loading of cargo proteins into autophagic vesicles at the phagophore assembly site (Yorimitsu and Klionsky, 2005), whereas Atg19 also becomes incorporated in autophagosomes destined for the vacuole. Given that impairment of autophagy could lead to greater accumulation of stress granule/autophagy intermediates, we further examined colocalization of Pub1-mCh and Atg19-GFP in a *mon1Δ* strain (which should impair autophagy prior to autophagosome/vacuole fusion) and in the *atg15Δ* strain (which results in IVCs). Importantly, we saw an increased colocalization of Pub1 with Atg19 in the *mon1Δ* background and could also observe clear colocalization of Atg19 with Pub1 in IVCs in the *atg15Δ* background (Figure S6; Table S4), arguing that colocalization is a consequence of a transient interaction of stress granules with autophagosomes for targeting to the vacuole.

We also observed that stress granules accumulated in an *ubx2Δ* strain, whereas the *vms1Δ* strain exhibited decreased P bodies (Table S2). Ubx2 and Vms1 both interact with Cdc48, the yeast ortholog of VCP, which is an AAA-ATPase that can promote autophagy (Krick et al., 2010; Meyer et al., 2012), including targeting of large ribosomal subunits for ribophagy (Ossareh-Nazari et al., 2010). These observations suggested that Cdc48 might also be important in targeting stress granules and/or P bodies for autophagy. To test this possibility, we examined the effects of a conditional allele of Cdc48 with a previously described autophagy defect (Krick et al., 2010) upon the accumulation of stress granules in yeast cells. We observed that at the restrictive temperature, Cdc48 inactivation led to the strong accumulation of stress granules, suggesting that Cdc48 plays a role in stress granule clearance (Figure 2B). Although the phenotype was not as strong as in the Cdc48 allele, we also observed increased stress granules in conditional alleles of the Cdc48-interacting proteins Ufd1 and Npl4 (Figure 2B; Table S4), suggesting these proteins can also affect the dynamics of stress granules.

Epistasis Tests Define a Pathway of Targeting Stress Granules to Vacuoles

The Cdc48 protein could affect stress granule dynamics in multiple manners. Cdc48 uses the energy of ATP hydrolysis to rearrange complexes containing ubiquitinated proteins (Stolz et al.,

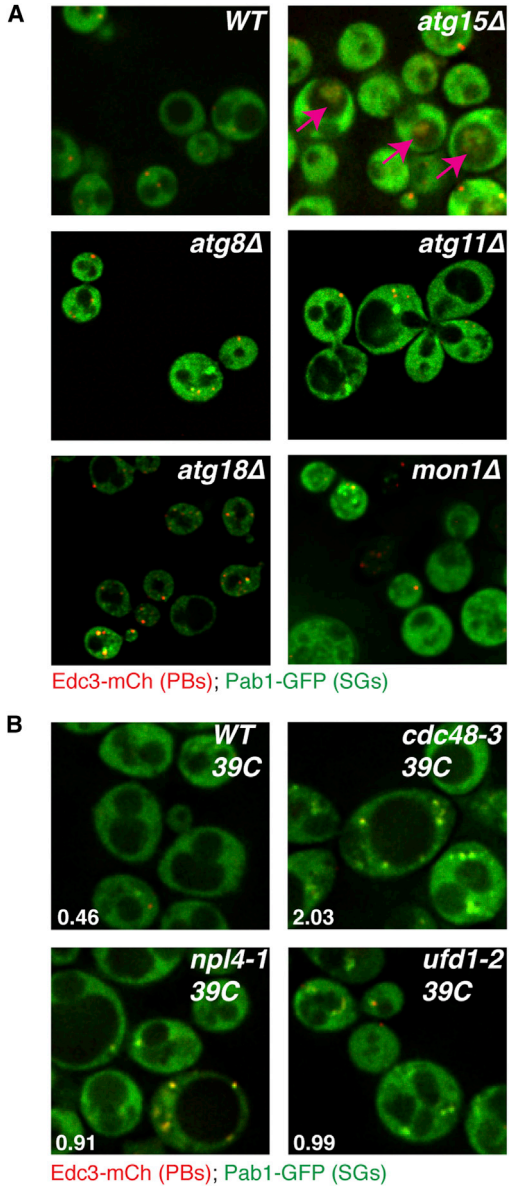

Figure 2. Several Autophagy and Cdc48-Complex Factors Exhibit Stress Granule Phenotypes

(A) Logarithmically growing strains lacking autophagy factors exhibit accumulation and/or mislocalization of stress granule and P body proteins.

(B) W303 strain background temperature-sensitive alleles of Cdc48, Ufd1, and Npl4 exhibit increased stress granules relative to WT at the nonpermissive temperature. Numbers indicate the average number of stress granule foci/cell in each strain, based on three independent experiments.

See also Figures S4, S5, and S6 and Table S4.

2011) and can function in targeting proteins to the proteasome (e.g., Meyer et al., 2012; Stolz et al., 2011), as well as promoting autophagy (Krick et al., 2010; Meyer et al., 2012; Ossareh-Nazari et al., 2010). To determine if Cdc48 affected autophagy of mRNP granules, we investigated how inactivation of Cdc48, or other autophagy genes, affected the formation of IVCs containing stress granule or P body markers in the *atg15Δ* strain. If Cdc48 is required for autophagy of stress granules and/or P bodies, we would expect a decrease in IVCs containing these components in a Cdc48-inactivated *atg15Δ* strain as compared to *atg15Δ* alone. Conversely, if Cdc48 affects stress granules by an unrelated mechanism, then the IVC compartments should be unchanged upon inactivation of Cdc48 activity.

This analysis of *atg15Δ* double mutants revealed two important observations. First, we observed that deletion of *ATG8*, *ATG11*, or *MON1*, which promote autophagy (Wang et al., 2002; Yorimitsu and Klionsky, 2005), significantly reduced the accumulation of stress granule markers within IVCs in the *atg15Δ* background (Figures 3A and 3B). Second, we observed that the temperature-sensitive *cdc48-3* allele led to a significant and progressive decrease in IVC levels following a 1 or 2 hr shift to the restrictive temperature, whereas IVC levels in the *atg15Δ* control cells actually elevated slightly under identical conditions (Figures 3C and 3D). IVC levels were already slightly reduced in the *cdc48-3 atg15Δ* strain prior to temperature shift, possibly suggesting partial loss of function, and stress granules were more abundant relative to *atg15Δ* control cells, consistent with a role for Cdc48 in their clearance. We interpret these observations to indicate that stress granules can be targeted to the vacuole in a process that is dependent on the autophagy machinery and Cdc48. We refer to this targeting of mRNP granules to the autophagic pathway as granulophagy to distinguish this process from nonspecific macroautophagy and other forms of selective autophagy. Moreover, because inactivation of Cdc48 activity reduces the accumulation of IVCs in the *atg15Δ* strain, this argues that Cdc48 enhances the targeting of stress granules to autophagy.

Targeting of RNP Granules by Autophagy Increases when mRNA Decay Is Inhibited

The targeting of stress granules and possibly P bodies to autophagy provides another mechanism regulating the clearance of these structures. This is in addition to translation initiation, which can reduce P bodies and stress granules by promoting the return of mRNAs to translation (Brengues et al., 2005; Bhattacharyya et al., 2006), as well as decapping and 5′ to 3′ degradation, which can reduce the mRNAs present within P bodies (Sheth and Parker, 2003). Because these RNP granules can have multiple fates, it suggests that decreases in one of these pathways would increase others. For example, we hypothesized that decreases in decapping or 5′ to 3′ exonucleolytic degradation, which lead to the accumulation of P bodies, stress granules, and a pool of nondegraded mRNAs (Sheth and Parker, 2003; Buchan et al., 2008) might lead to an increased flux of mRNPs into autophagy. To test this prediction, we analyzed the amount of IVCs accumulating in an *atg15Δ* strain carrying the *xrn1Δ* deletion or a temperature-sensitive allele of the decapping enzyme (*dcp2-7*). Strikingly, compared to the *atg15Δ* strain, we observed an increase in both the number of cells with IVC compartments and the relative size and intensity of the IVC in *xrn1Δ atg15Δ* strains, and in the *dcp2-7 atg15Δ* strain after a shift to the restrictive temperature (Figure 4). This observation provides additional evidence that stress granules can be targeted for autophagy and suggests that this pathway increases when mRNA decay is blocked and the cell has accumulated a larger pool of RNP granules.

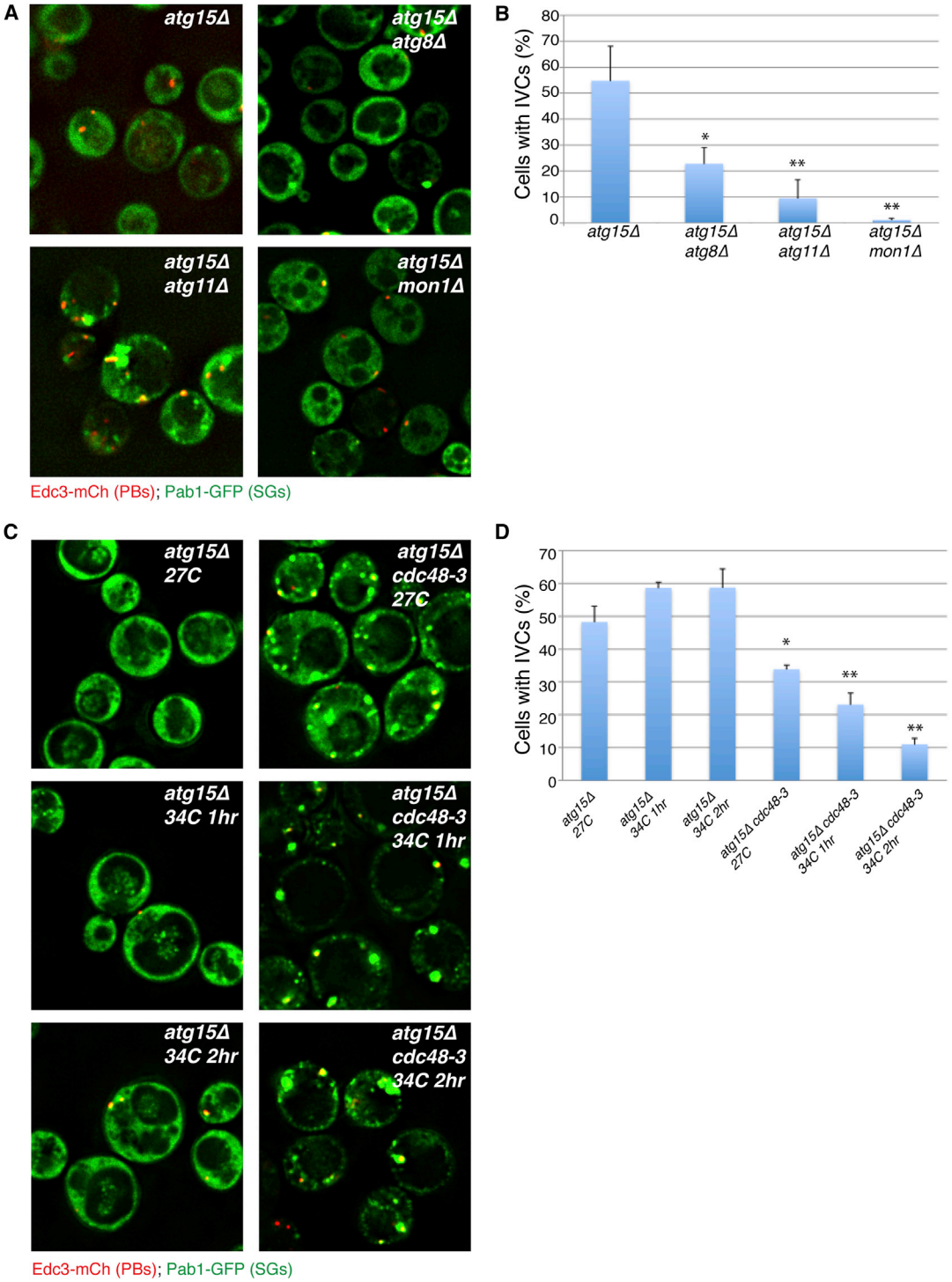

Figure 3. *Atg15Δ*-Induced IVCs Are Decreased by Upstream Mutations in Autophagy Pathways and in Cdc48

(A) BY4741 background strains in early stationary phase. IVCs present in an *atg15Δ* strain are reduced by secondary mutations in autophagy factors acting at/prior to autophagosome-vacuolar membrane fusion.

(B) Quantitation of data in (A). Mean values are based on three independent experiments ± SD. *$p < 0.05$; **$p < 0.005$) relative to *atg15Δ* indicated.

(C) W303 strain background, examined in early stationary phase following 0, 1, or 2 hr of 34°C heat shock. Inactivation of Cdc48 results in decreased IVCs caused by atg15 deletion.

(D) Quantitation of data in (C). Mean values are based on a minimum of three replicate experiments ± SD. p values as above.

See also Table S4.

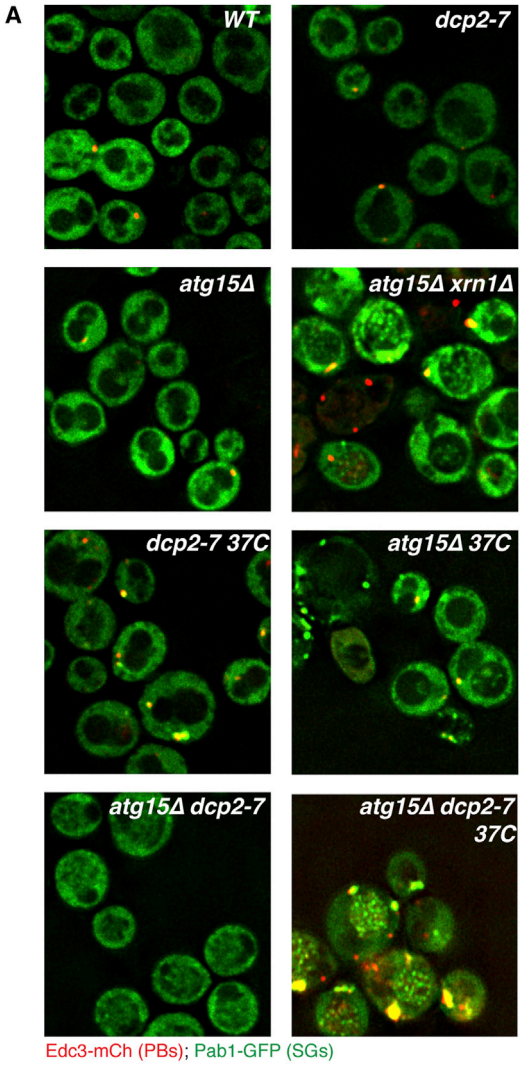

Figure 4. Impairment of Cytoplasmic mRNA Decay Increases Accumulation of Granule Proteins in IVCs

(A) RP840-background strains in early stationary phase. Temperature shifted strains were subject to 1 hr at 37°C (lower row).

(B) Quantitation of data in (A). Mean values are based on a minimum of three replicate experiments ± SD. *$p < 0.05$, **$p < 0.005$) relative to *atg15Δ* indicated. See also Table S4.

Autophagy Affects Stress Granule Clearance in Mammalian Cells

The conservation of P bodies, stress granules, and the autophagic process implies that mRNP granules would also be targeted for autophagy in other eukaryotic cells. This model predicts that inhibiting autophagy in mammalian cells would lead to the accumulation of constitutive stress granules and would reduce the rate at which they are cleared following removal of a stress. To test this possibility, we examined stress granules in mouse embryonic fibroblasts (MEFs) bearing homozygous deletion of *ATG7* both in the absence of stress and following relief of a stress.

Examination of endogenous stress granule components revealed two observations arguing that autophagy affects the rate of stress granule clearance. First, in the absence of any stress we observed that $Atg7^{-/-}$ MEFs showed a small but consistent percentage of cells with clearly visible stress granules, whereas corresponding wild-type MEFs cells showed no cells with stress granules (Figures 5A, 5D, and 5E); a similar result was also observed in $Atg3^{-/-}$ MEF lines (Figure S7C). Second, we observed that whereas stress granules formed robustly in both wild-type and $Atg7^{-/-}$ MEFs in response to a heat shock (Figures 5B and 5D), the majority of the stress granules were cleared from wild-type MEFs upon return to 37°C, while persisting in $Atg7^{-/-}$ MEFs for up to 2 hr (Figures 5C and 5D). These observations argue that at least a subset of stress granules are cleared by autophagy in mammalian cells. Consistent with that interpretation, we observe that autophagy-promoting drugs (either rapamycin or 3-MA; Wu et al., 2010) enhance the clearance of arsenite-induced stress granules (Figures S7A and S7B). By contrast, the autophagy inhibitor wortmannin attenuates stress granule clearance (Figures S7A and S7B).

VCP Affects Stress Granule Clearance in Mammalian Cells

The effect of Cdc48 on stress granules in yeast suggested that the mammalian ortholog VCP might play a role in stress granule clearance. To test this hypothesis, we depleted VCP function in mammalian cells either by small interfering RNA (siRNA) or by chemical inhibition of VCP activity and examined the formation and clearance of stress granules during heat shock and recovery. We observed that either siRNA knockdown (Figures 6A–6D) or chemical inhibition of VCP in HeLa cells (Figures 6E and 6F) led to significantly reduced stress granule clearance, indicating that VCP is required for efficient stress granule clearance in mammalian cells. Moreover, because endogenous VCP accumulates in stress granules during different stress conditions (heat stress, osmotic stress, oxidative stress; Figure 7A), the simplest model is that VCP directly acts on stress granules to promote their clearance.

The requirement of VCP for stress granule clearance in mammalian cells raised the possibility that disease-causing mutations in VCP might impair stress granule dynamics. Indeed, VCP-related diseases, including ALS, FTLD, and MSP, are all

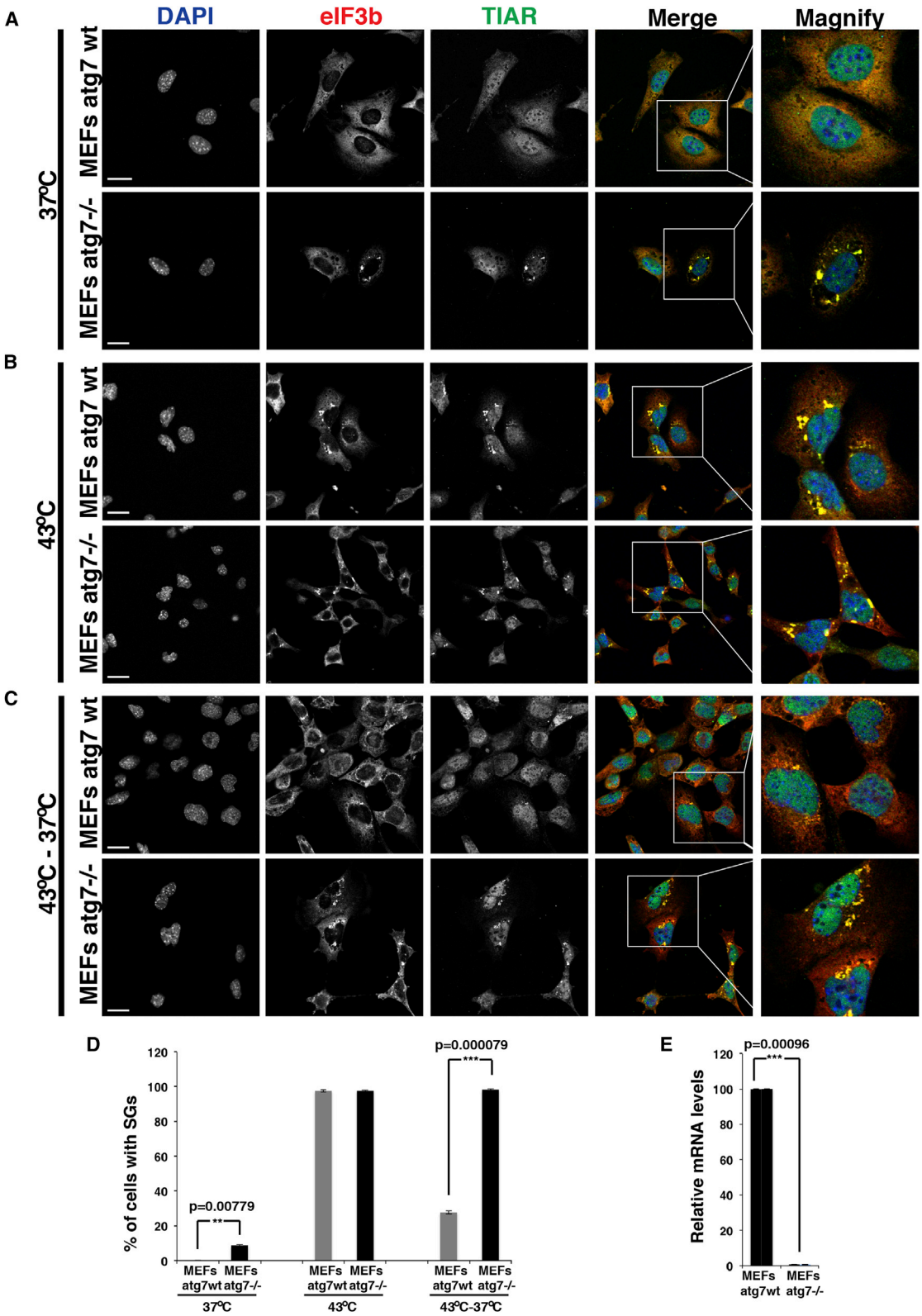

(legend on next page)

characterized by accumulation of cytoplasmic inclusions of stress granule constituents TDP-43, hnRNPA1, and/or hnRNPA2 (Neumann et al., 2006, 2007; Salajegheh et al., 2009; Kim et al., 2013). Strikingly, we observed that HeLa cells overexpressing the VCP disease-related mutations A232E and R155H showed the constitutive appearance of stress granules containing eIF3 subunits TDP-43 and VCP itself (Figure 7D). The accumulation of constitutive stress granules in cells expressing pathological alleles of VCP is consistent with the hypothesis that impaired stress granule dynamics may be a shared defect underlying the pathogenesis of disease initiated by mutations in VCP as well as disease initiated by stress-granule-promoting mutations in RNA-binding proteins TDP-43, FUS, hnRNPA1, and hnRNPA2B1.

DISCUSSION

In this work, we identified over 100 genes that are involved in the modulation of stress granules and/or P bodies in yeast. These proteins show a dense network of physical and genetic interactions indicating they reveal a previously unknown network of proteins controlling mRNP granule dynamics. Given the role of RNP granules in translation and mRNA degradation, it was not unexpected that this set of proteins would contain multiple factors involved in mRNA biogenesis and function (Edc2, Lsm6, Mlp1, Pap2, Rnh70, Rpl35b, Rpl39, Rpl42a, Rps28b, Sto1, Tif3, Trm12, Sro9, and Xrn1). Surprisingly, we also observed that defects in the THO or TREX-2 complexes led to the constitutive formation of stress granules, perhaps because some newly exported mRNAs are deficient at entering translation. Another interesting concentration of mutants included defects in the prefoldin complex, which decreased P bodies, and could reflect a failure to properly assemble cytoskeletal structures to which mRNP granule assembly and trafficking has been linked (Aizer et al., 2008; Loschi et al., 2009). Mutants affecting various signaling pathways (e.g., Kcs1, Cmk1, Mds3) and intriguing cellular processes (e.g., chromatin modification/assembly: Gcn5, Hst1, Iki3, Isw1, Rlf2, Set2, Swc5, Swd3, and Swr1) were also observed. An important area of future research will be to understand how these proteins affect RNA-granule dynamics in molecular detail, and the physiological consequences of such aberrant assembly.

Analysis of these mutants provided several lines of evidence that yeast stress granules and P bodies can be targeted to the vacuole by autophagy. First, mutations that inhibit autophagy at stages prior to autophagosome-vacuolar membrane fusion accumulated stress granules (Figure 2), which is consistent with stress granules continually being cleared by an autophagic process. Second, strains deficient in the Atg15 lipase, which breaks down autophagic vesicles within the vacuole, accumulate stress granule and P body markers in IVCs, consistent with the accumulation of autophagic vesicles in the *atg15Δ* strain (Figure 2). Third, combining the *atg15Δ* deletion with earlier blocks to autophagy decreases the accumulation of stress granule and P body markers in IVCs and often increases the cytoplasmic accumulation of stress granules (Figure 3). Fourth, when decapping or 5′ to 3′ mRNA degradation is inhibited, which leads to increased levels of mRNP granules, we observed an even greater accumulation of stress granule markers within IVCs in *atg15Δ* strains (Figure 4). This argues that the targeting of RNP granules to autophagy is increased in the absence of normal levels of mRNA degradation. Taken together, we conclude that stress granules and P bodies, and presumably the mRNAs within them, can be targeted to vacuoles by autophagy. We refer to this targeting of mRNP granules to the autophagic pathway as granulophagy to distinguish this process from nonspecific macroautophagy and other forms of selective autophagy.

Several observations suggest that yeast stress granules are more commonly targeted for granulophagy than P bodies. First, mutants defective in autophagy show a greater increase in stress granules than P bodies (Table S2). Second, in *atg15Δ dcp2-7* and *atg15Δ xrn1Δ* mutants, which show an accumulation of both P bodies and stress granules, we see a greater accumulation of the stress granule marker Pab1 in vacuoles than the P body component Edc3 (Figure 4). Third, our analyses to date have determined four known stress granule factors within *atg15Δ* IVCs (Pab1, Pub1, Pbp1, and Ded1; Figure S5), whereas only Edc3 has been observed at a modest level; Dcp2 and Lsm1 are not detected in IVCs (data not shown). One possible model to explain the bias in targeting stress granules for autophagy is that mRNPs within P bodies either can also be degraded or can undergo mRNP remodeling to enter stress granules (Buchan et al., 2008). Thus, if autophagy is generally slow compared to these events, then most mRNPs will transition to a stress-granule type of mRNP before being targeted for autophagy.

Several observations suggest that the targeting of stress granules to degradative organelles by autophagy is conserved in eukaryotes including mammals. First, MEFs defective in autophagy show a low level of constitutive stress granules, consistent with a defect in stress granule resolution (Figures 5A and S7C). Second, Atg7$^{-/-}$ MEFs are defective in clearing stress granules after relief of heat stress (Figures 5B–5D). Third, we observed that 3-MA and to a lesser extent rapamycin, which can stimulate autophagy (Wu et al., 2010), increased the rate at which stress granules were cleared following the relief of oxidative stress (Figures S7A and S7B). In contrast, inhibition of autophagy by wortmannin slowed the rate of stress granule

Figure 5. Mammalian Stress Granule Clearance Is Impaired by Defective Autophagy

(A) Atg7$^{-/-}$ MEFs showed a low level of cells with clearly visible stress granules even in the absence of exogenous stressors.

(B) Heat shock for 1 hr at 43°C resulted in robust stress granule formation in both WT and Atg7$^{-/-}$ MEFs.

(C) After shift from 43°C back to 37°C, stress granules clear within minutes in wild-type MEFs but persist for the duration of the assay (2 hr) in Atg7$^{-/-}$ MEFs. Scale bar equals 10 μm.

(D) Quantitation of the data in (A)–(C). Mean values are based on a minimum of three replicate experiments ± SEM.

(E) Real-time quantitative PCR verifies the expression levels of Atg7 in wild-type and Atg7$^{-/-}$ MEFs.

See also Figure S7.

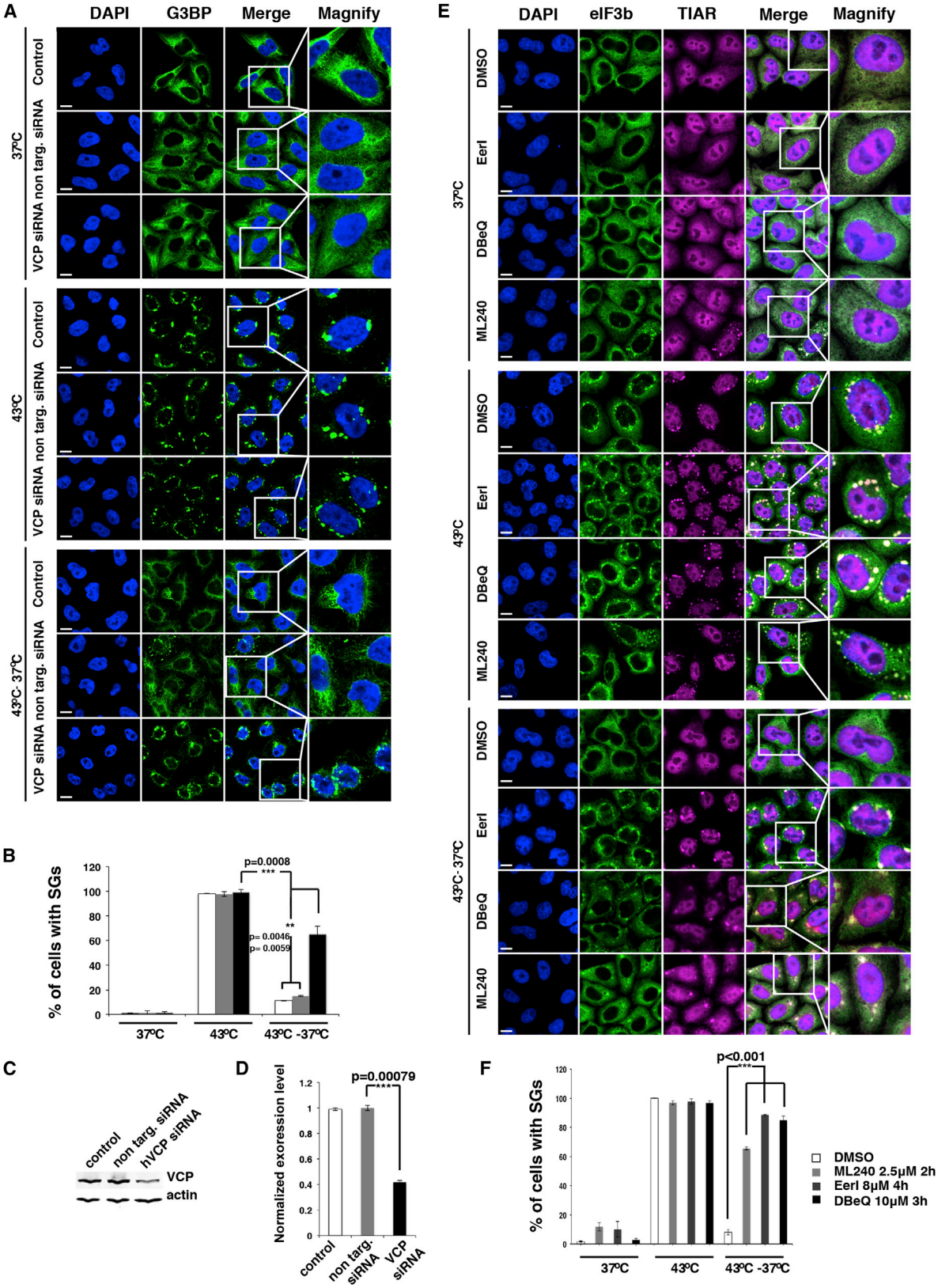

(legend on next page)

clearance (Figures S7A and S7B). Fourth, inhibition of the vacuolar ATPase function, either by mutations in yeast or pharmacologically in mammalian cells, leads to increases in stress granules (Tables S2 and S4; Figure S7D). This is relevant because vacuolar ATPases have been implicated in a wide array of vesicular trafficking events, often independent of proton-pumping activity, including maturation and fusion of autophagosomes with the lysosome in mammals (Klionsky et al., 2008), vacuole-vacuole fusion (Peters et al., 2001), and phagosome-lysosome fusion (Peri and Nüsslein-Volhard, 2008). Finally, in *C. elegans* it has been suggested that P granules, which are RNP granules related to stress granules, and P bodies can be cleared from blastomeres by autophagy (Zhang et al., 2009).

The autophagic degradation of stress granules and P bodies provides an additional fate for the mRNPs that accumulate within these structures. Such a fate might be particularly important for mRNPs within stress granules, which can also return to translation, and might serve an important role in modulating the stress response, particularly during prolonged stress, where stress-granule-associated mRNPs unable to return to translation might instead be targeted for vacuole/lysosome-based degradation. Moreover, this pathway provides a novel mechanism by which eukaryotic mRNAs could degrade, and one anticipates that for a subset of mRNAs this is a prevalent pathway by which they are degraded. Indeed, such a pathway could explain why miRNA-based mRNA degradation is affected by alterations in membrane flow given that miRNA-based repression machinery associates with endosomal compartments (Gibbings et al., 2009). Related to this, Ago2 and Dicer appear to be targeted by selective autophagy, with resulting consequences on miRNA-based repression (Gibbings et al., 2012).

Several observations also argue that Cdc48 and its mammalian ortholog VCP function in stress granule clearance. First, temperature-sensitive alleles of Cdc48, as well as mutations in the associated Ubx2, Npl4, and Ufd1 proteins, showed an accumulation of stress granules (Figure 2; Table S4). Second, depletion of VCP activity in tissue culture cells with either siRNAs or VCP inhibitors leads to a defect in the clearance of stress granules (Figure 6). Third, pathogenic mutations in *VCP* lead to constitutive accumulation of stress granules in cells in culture (Figure 7), which contain TDP-43, the major defining constituent of pathological cytoplasmic inclusions in patients with ALS, FTLD, IBM, and MSP (Neumann et al., 2006, 2007; Salajegheh et al., 2009; Kim et al., 2013). Taken together, these observations demonstrate Cdc48/VCP is required for efficient stress granule clearance, and this function may be relevant to its role in pathologies.

An unresolved role is the specific function of Cdc48/VCP in stress granule clearance. Because inhibition of Cdc48 function reduces the presence of stress granules in the IVCs in the *atg15Δ* background (Figure 3), we suggest that at least part of Cdc48's function in yeast is to promote autophagy of these mRNP granules. Ubiquitination is likely to be involved in modulating stress granules and P body dynamics because Cdc48/VCP utilizes ATP hydrolysis to segregate ubiquitinated proteins from a variety of cellular complexes (Stolz et al., 2011), stress granules in mammalian cells are heavily ubiquitinated (Kwon et al., 2007), and we observed that deletion of an E3 ubiquitin ligase of unknown function, Hel2, leads to increased stress granules (Table S2). In addition, autophagic clearance of ubiquitinated protein aggregates by VCP is facilitated by its known binding partner HDAC6, which itself binds ubiquitinated proteins and also regulates stress granule assembly in mammalian cells (Ju et al., 2008; Kwon et al., 2007). Because VCP accumulates within stress granules (Figure 7), one possible model is that the Cdc48/VCP complex works on some ubiquitinated component of stress granules to alter the mRNP complexes in a manner that promotes disassembly and/or targeting of the RNP granule to autophagy. However, ubiquitin may also affect stress granule dynamics through the proteasome because we identified mutations in the *PRE9* and *POC4* genes, which affect proteasome function, as increasing constitutive stress granules (Table S2), and inhibiting proteasome activity in mammals induces stress granules (Mazroui et al., 2007).

Our observations have important implications for the understanding of the role of RNP aggregates in some degenerative diseases. First, the targeting of stress granules to vacuoles/lysosome for degradation implies that aberrant forms of these granules that accumulate in some degenerative diseases, such as ALS, FTLD, IBM, and MSP, may also be cleared by this process. Notably, TDP-43, the most consistently observed component of pathological cytoplasmic inclusions in ALS, FTLD, and MSP, is preferentially cleared by autophagy (Wang et al., 2010, 2012). Consistent with this notion, Cdc48 inactivation was also recently shown to enhance TDP-43 toxicity in a yeast neurodegenerative model system (Armakola et al., 2012). Thus, mechanisms to enhance autophagy of stress granules and related RNP aggregates may have potential as therapies to treat various degenerative diseases.

These results also strengthen the hypothesis that ALS, FTLD, and some related pathologies arise due to hyperformation or stabilization of stress granules. This was first suggested by the observations that mutations in the stress granule components TDP-43, FUS, hnRNPA1, hnRNPA2, and Atx2 that enhanced

Figure 6. VCP Is Essential for Stress Granule Clearance

(A) HeLa cells examined by immunofluorescence for the stress granule marker G3BP. Cells treated with nontargeting siRNA show stress granule assembly upon heat shock at 43°C (2 hr) and rapid clearance of stress granules upon return to 37°C. Cells treated with VCP-targeting siRNA show normal stress granule assembly, but these stress granules fail to clear following return to 37°C (2 hr). Scale bar equals 10 μm.

(B) Quantification of data in (A). Mean values are based on a minimum of three replicate experiments ± SEM.

(C and D) Western blot and quantification of VCP protein levels in cells from (A). Mean values are based on a minimum of three replicate experiments ± SEM.

(E) HeLa cells examined by immunofluorescence for the stress granule markers TIAR and eIF3b. Pretreatment with chemical inhibitors of VCP impairs clearance of stress granules. Cells were treated with vehicle (DMSO) or specific inhibitors Eer1 (4 hr pretreatment with 8 μM Eeyarestatin I, per Wang et al., 2010); DBeQ (3 hr pretreatment with 10 μM DBeQ, per Chou et al., 2011); ML240 (2 hr pretreatment with 2.5 μM ML240, per Chou et al., 2013). Scale bar equals 10 μm.

(F) Quantification of the data in (E). Mean values are based on a minimum of three replicate experiments ± SEM.

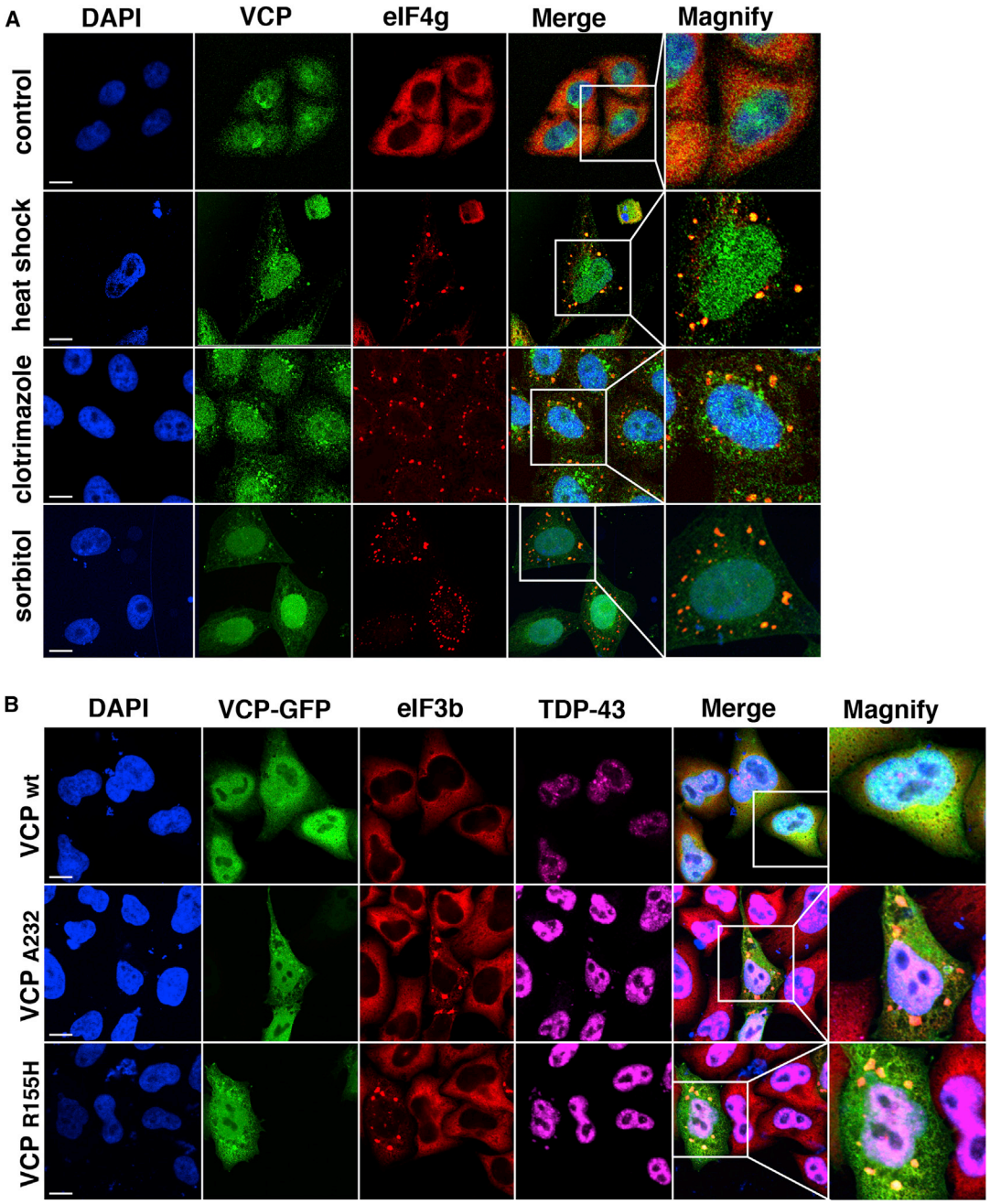

Figure 7. VCP Is Recruited to Stress Granules and Disease-Causing Mutations in *VCP* Induce Constitutive Stress Granules that Contain the Disease Protein TDP-43

(A) HeLa cells stained for endogenous VCP and the stress granule marker eIF4G. VCP is recruited to stress granules induced by three distinct stimuli: heat shock at 43°C for 2 hr, incubation with 20 μM clotrimazole for 1 hr, or incubation with 0.6 M sorbitol for 1 hr. Scale bar equals 10 μm.

(B) HeLa cells transfected with plasmid expressing wild-type or mutant (A232E and R155H) VCP-GFP and stained for eIF3b and TDP-43. Overexpression of mutant but not wild-type VCP results in the formation of constitutive stress granules that contain the disease protein TDP-43. Scale bar equals 10 μm.

their self-assembly or aggregation could be causative in these diseases as well as causing the accumulation of stress granules or related RNP aggregates in model systems as well as patient tissue (Kim et al., 2013; Dewey et al., 2012; Ito and Suzuki 2011). Strikingly, *VCP* mutations lead to the same spectrum of pathologies as the aggregation-prone mutations in these RNA binding proteins. Given a role for VCP/Cdc48 in stress granule clearance, and pathological mutations in *VCP* leading to the constitutive appearance of stress granules, we suggest that the pathologies of *VCP* mutations and hyperaggregation

mutations in RNA binding proteins are similar because they both lead to the accumulation and/or persistence of stress granules. This also raises the exciting possibility that mutations we have identified in yeast that lead to the formation of constitutive stress granules may identify candidate genes that, when mutated in humans, contribute to the formation of both constitutive stress granules in mammalian cells and degenerative disease.

EXPERIMENTAL PROCEDURES

Yeast Microscopy

For the screen, deletion strain and WT control transformants were inoculated overnight in 300 μl of selective minimal media in 96-well plates and agitated at 30°C for optimal growth. The following morning, staggered reinoculation at OD_{600}s of <0.1, followed by growth to an approximate OD_{600} of 0.5, was conducted. Samples were spotted onto 8-well Teflon-coated slides (Tekdon), coverslips were sealed with nail varnish, and cells were imaged using a Deltavision RT microscope with 100× objective (Applied Biosystems). Two images were collected for each strain at 2 × 2 binning, resulting in the capture of approximately 50–100 cells. Manual imaging, blind to gene identity, ensured both high-quality data sets and helped detect phenotypes that are hard to quantify with automated algorithms. Because nonstressed yeast cells exhibit virtually no stress granules and have reasonable numbers of semibright P bodies, deletion strains exhibiting stress granule induction or P body induction/reduction phenotypes were easily distinguished. Strains identified with a phenotype were rescreened blindly as above, and only those with repeating phenotypes made the final list (more detail on phenotype classification is in Extended Experimental Procedures).

Additional microscopy analysis was conducted using the above system, a Deltavision Elite system with 100× objective (Applied Biosystems), and a Nikon A1R Confocal operating in wide-field mode, also with a 100× objective (Nikon). Yeast strains were examined either in logarithmic grow (OD_{600} 0.4–0.5) or in early stationary phase (inoculation at OD_{600} 0.2 followed by growth for 18–24 hr). Entry into early stationary phase was ensured for each strain with OD_{600} measurements and prior knowledge of a given strain's maximal OD_{600} in minimal media culture. Examination under such conditions maximized detection of IVCs in an *atg15Δ* background. Details of yeast transformation, strain identification, and image analysis are in Extended Experimental Procedures. All yeast strains utilized in this study are detailed in Table S5.

Bioinformatic Analysis

Cytoscape v 2.8.2 (Smoot et al., 2011) and the *S. cerevisiae* Biogrid interaction data set 3.1.86 (http://wwww.thebiogrid.org) were used to plot network and subnetwork analyses of the known physical and genetic interactions of the 125 screen hits. Significance of the resulting 100 node, 448 nonredundant interaction network was determined by simulation analysis using 125 randomly selected genes from the 4,249 strains transformed in the screen, and plotting networks using identical parameters to the above. The average values for 100 random networks exhibited a Gaussian distribution, with means of 47.8 ± 11.8 nodes and 77.6 ± 25.7 nonredundant interactions. Z score analysis confirmed our screen network to be significant (p value 5.34×10^{-6}). GO term classification was obtained at the *S. cerevisiae* database (http://www.yeastgenome.org).

HeLa and MEF Cell Growth Conditions and Fixation

HeLa cells, incubated in a 37°C incubator with a 5% CO_2 concentration, were grown in DMEM media (Gibco or HyClone) supplemented with 10% FBS (Atlas Biological or HyClone), 2 mM L-GlutaMAX (Gibco), and Pen-Strep (100 U/ml penicillin, 100 μg/ml streptomycin; Gibco). Prior to analysis, cells were passaged from flasks onto 8-well chamber slides (Nalge Nunc) or 4-well and 8-well slides (Millipore), and grown for 1.5–2 days to reach 60%–70% confluency. For details on HeLa cell drug additions, see Extended Experimental Procedures. During stress granule clearance experiments, cells were subject to a 1 hr arsenite stress. This was followed by washing in fresh media, followed by resuspension in fresh media alone, or in the additional presence of a drug, and fixation at 20 min, 1 hr, 2 hr, and 3 hr time points. Paraformaldehyde fixation of cells was as described in Kedersha and Anderson (2007).

$Atg3^{-/-}$ MEF cells were grown similarly to HeLa, but in media containing sodium pyruvate (Gibco) and nonessential amino acids (Sigma), while lacking GlutaMAX. Fixation protocols were as above. $Atg7^{-/-}$ MEF cells were grown in DMEM (HyClone) 10% FBS (HyClone) and GlutaMax-1x (Gibco). The cells were fixed in 4% paraformaldehyde (Electron Microscopy Science). Transfection details are in Extended Experimental Procedures.

HeLa and MEFs Immunofluorescence and Microscopy

Antibodies and concentrations used in HeLa and MEF cell immunofluorescence are detailed in Extended Experimental Procedures. Slides were mounted using Vectashield with DAPI (Vector Laboratories) or ProLong Gold Antifade Reagent with DAPI (Invitrogen; P3691). Images were captured using a Nikon A1R Confocal microscope (Nikon) using a 100× objective or a LSM510 (Zeiss) confocal microscope with a 63× objective. All images are collapsed z stacks (7 μM depth, 0.25 μM slices). Stress granules were quantified on a percentage cell basis, whereas cells deemed to have P bodies required foci to be above a threshold intensity value. $Atg3^{-/-}$ MEFs were stained as above, but imaged on a Deltavision Elite system (Applied Biosystems) using a 100× objective.

SUPPLEMENTAL INFORMATION

Supplemental Information includes Extended Experimental Procedures, seven figures, and five tables and can be found with this article online at http://dx.doi.org/10.1016/j.cell.2013.05.037.

ACKNOWLEDGMENTS

We thank the Chen lab (Institute of Molecular Biology, Taiwan) for Cdc48, Ufd1, and Npl4 conditional allele strains, the Klionsky lab (University of Michigan) for a GFP-Atg19 expressing plasmid, the Komatsu lab (Tokyo Metropolitan Institute of Medical Sciences) for Atg $3^{-/-}$ MEF cell lines, and the Green lab (St. Jude Children's Research Hospital) for $Atg7^{-/-}$ MEF cell lines. We also thank the Cell and Tissue Imaging Core Facility at St. Jude Children's Research Hospital and all Parker lab members for feedback, particularly Saumya Jain for bioinformatics assistance. This work was supported by funds from the ALS Association to R.-M.K., the Packard Center for ALS Research to J.P.T., and the Howard Hughes Medical Institute to J.R.B. and R.P.

Received: December 14, 2012
Revised: March 26, 2013
Accepted: May 20, 2013
Published: June 20, 2013

REFERENCES

Aizer, A., Brody, Y., Ler, L.W., Sonenberg, N., Singer, R.H., and Shav-Tal, Y. (2008). The dynamics of mammalian P body transport, assembly, and disassembly in vivo. Mol. Biol. Cell *19*, 4154–4166.

Anderson, P., and Kedersha, N. (2009). RNA granules: post-transcriptional and epigenetic modulators of gene expression. Nat. Rev. Mol. Cell Biol. *10*, 430–436.

Arimoto, K., Fukuda, H., Imajoh-Ohmi, S., Saito, H., and Takekawa, M. (2008). Formation of stress granules inhibits apoptosis by suppressing stress-responsive MAPK pathways. Nat. Cell Biol. *10*, 1324–1332.

Armakola, M., Higgins, M.J., Figley, M.D., Barmada, S.J., Scarborough, E.A., Diaz, Z., Fang, X., Shorter, J., Krogan, N.J., Finkbeiner, S., et al. (2012). Inhibition of RNA lariat debranching enzyme suppresses TDP-43 toxicity in ALS disease models. Nat. Genet. *44*, 1302–1309.

Beckham, C.J., and Parker, R. (2008). P bodies, stress granules, and viral life cycles. Cell Host Microbe *3*, 206–212.

Bhattacharyya, S.N., Habermacher, R., Martine, U., Closs, E.I., and Filipowicz, W. (2006). Stress-induced reversal of microRNA repression and mRNA

P-body localization in human cells. Cold Spring Harb. Symp. Quant. Biol. *71*, 513–521.

Brengues, M., Teixeira, D., and Parker, R. (2005). Movement of eukaryotic mRNAs between polysomes and cytoplasmic processing bodies. Science *310*, 486–489.

Buchan, J.R., and Parker, R. (2009). Eukaryotic stress granules: the ins and outs of translation. Mol. Cell *36*, 932–941.

Buchan, J.R., Muhlrad, D., and Parker, R. (2008). P bodies promote stress granule assembly in Saccharomyces cerevisiae. J. Cell Biol. *183*, 441–455.

Chou, T.F., Brown, S.J., Minond, D., Nordin, B.E., Li, K., Jones, A.C., Chase, P., Porubsky, P.R., Stoltz, B.M., Schoenen, F.J., et al. (2011). Reversible inhibitor of p97, DBeQ, impairs both ubiquitin-dependent and autophagic protein clearance pathways. Proc. Natl. Acad. Sci. USA *108*, 4834–4839.

Chou, T.F., Li, K., Frankowski, K.J., Schoenen, F.J., and Deshaies, R.J. (2013). Structure-activity relationship study reveals ML240 and ML241 as potent and selective inhibitors of p97 ATPase. ChemMedChem *8*, 297–312. http://dx.doi.org/10.1002/cmdc.201200520.

Decker, C.J., Teixeira, D., and Parker, R. (2007). Edc3p and a glutamine/asparagine-rich domain of Lsm4p function in processing body assembly in Saccharomyces cerevisiae. J. Cell Biol. *179*, 437–449.

Dewey, C.M., Cenik, B., Sephton, C.F., Johnson, B.A., Herz, J., and Yu, G. (2012). TDP-43 aggregation in neurodegeneration: are stress granules the key? Brain Res. *1462*, 16–25.

Didiot, M.C., Subramanian, M., Flatter, E., Mandel, J.L., and Moine, H. (2009). Cells lacking the fragile X mental retardation protein (FMRP) have normal RISC activity but exhibit altered stress granule assembly. Mol. Biol. Cell *20*, 428–437.

Doyle, M., and Kiebler, M.A. (2011). Mechanisms of dendritic mRNA transport and its role in synaptic tagging. EMBO J. *30*, 3540–3552.

Erickson, S.L., and Lykke-Andersen, J. (2011). Cytoplasmic mRNP granules at a glance. J. Cell Sci. *124*, 293–297.

Franks, T.M., Singh, G., and Lykke-Andersen, J. (2010). Upf1 ATPase-dependent mRNP disassembly is required for completion of nonsense-mediated mRNA decay. Cell *143*, 938–950.

Gibbings, D.J., Ciaudo, C., Erhardt, M., and Voinnet, O. (2009). Multivesicular bodies associate with components of miRNA effector complexes and modulate miRNA activity. Nat. Cell Biol. *11*, 1143–1149.

Gibbings, D., Mostowy, S., Jay, F., Schwab, Y., Cossart, P., and Voinnet, O. (2012). Selective autophagy degrades DICER and AGO2 and regulates miRNA activity. Nat. Cell Biol. *14*, 1314–1321.

Gilks, N., Kedersha, N., Ayodele, M., Shen, L., Stoecklin, G., Dember, L.M., and Anderson, P. (2004). Stress granule assembly is mediated by prion-like aggregation of TIA-1. Mol. Biol. Cell *15*, 5383–5398.

Ginsberg, S.D., Galvin, J.E., Chiu, T.S., Lee, V.M., Masliah, E., and Trojanowski, J.Q. (1998). RNA sequestration to pathological lesions of neurodegenerative diseases. Acta Neuropathol. *96*, 487–494.

Gkogkas, C., Sonenberg, N., and Costa-Mattioli, M. (2010). Translational control mechanisms in long-lasting synaptic plasticity and memory. J. Biol. Chem. *285*, 31913–31917.

Ito, D., and Suzuki, N. (2011). Conjoint pathologic cascades mediated by ALS/FTLD-U linked RNA-binding proteins TDP-43 and FUS. Neurology *77*, 1636–1643.

Johnson, J.O., Mandrioli, J., Benatar, M., Abramzon, Y., Van Deerlin, V.M., Trojanowski, J.Q., Gibbs, J.R., Brunetti, M., Gronka, S., Wuu, J., et al.; ITALSGEN Consortium. (2010). Exome sequencing reveals VCP mutations as a cause of familial ALS. Neuron *68*, 857–864.

Ju, J.S., Miller, S.E., Hanson, P.I., and Weihl, C.C. (2008). Impaired protein aggregate handling and clearance underlie the pathogenesis of p97/VCP-associated disease. J. Biol. Chem. *283*, 30289–30299.

Kato, M., Han, T.W., Xie, S., Shi, K., Du, X., Wu, L.C., Mirzaei, H., Goldsmith, E.J., Longgood, J., Pei, J., et al. (2012). Cell-free formation of RNA granules: low complexity sequence domains form dynamic fibers within hydrogels. Cell *149*, 753–767.

Kedersha, N., and Anderson, P. (2007). Mammalian stress granules and processing bodies. Methods Enzymol. *431*, 61–81.

Kim, N.C., Tresse, E., Kolaitis, R.M., Molliex, A., Thomas, R.E., Alami, N.H., Wang, B., Joshi, A., Smith, R.B., Ritson, G.P., et al. (2013). VCP Is Essential for Mitochondrial Quality Control by PINK1/Parkin and this Function Is Impaired by VCP Mutations. Neuron *78*, 65–80. http://dx.doi.org/10.1016/j.neuron.2013.02.029.

Klionsky, D.J., Elazar, Z., Seglen, P.O., and Rubinsztein, D.C. (2008). Does bafilomycin A1 block the fusion of autophagosomes with lysosomes? Autophagy *4*, 849–950.

Krick, R., Bremer, S., Welter, E., Schlotterhose, P., Muehe, Y., Eskelinen, E.L., and Thumm, M. (2010). Cdc48/p97 and Shp1/p47 regulate autophagosome biogenesis in concert with ubiquitin-like Atg8. J. Cell Biol. *190*, 965–973.

Kwon, S., Zhang, Y., and Matthias, P. (2007). The deacetylase HDAC6 is a novel critical component of stress granules involved in the stress response. Genes Dev. *21*, 3381–3394.

Leung, A.K., Calabrese, J.M., and Sharp, P.A. (2006). Quantitative analysis of Argonaute protein reveals microRNA-dependent localization to stress granules. Proc. Natl. Acad. Sci. USA *103*, 18125–18130.

Loschi, M., Leishman, C.C., Berardone, N., and Boccaccio, G.L. (2009). Dynein and kinesin regulate stress-granule and P-body dynamics. J. Cell Sci. *122*, 3973–3982.

Mazroui, R., Di Marco, S., Kaufman, R.J., and Gallouzi, I.E. (2007). Inhibition of the ubiquitin-proteasome system induces stress granule formation. Mol. Biol. Cell *18*, 2603–2618.

Medioni, C., Mowry, K., and Besse, F. (2012). Principles and roles of mRNA localization in animal development. Development *139*, 3263–3276.

Meyer, H., Bug, M., and Bremer, S. (2012). Emerging functions of the VCP/p97 AAA-ATPase in the ubiquitin system. Nat. Cell Biol. *14*, 117–123.

Mijaljica, D., Prescott, M., and Devenish, R.J. (2011). V-ATPase engagement in autophagic processes. Autophagy *7*, 666–668.

Mitchell, S.F., Jain, S., She, M., and Parker, R. (2013). Global analysis of yeast mRNPs. Nat. Struct. Mol. Biol. *20*, 127–133.

Neumann, M., Sampathu, D.M., Kwong, L.K., Truax, A.C., Micsenyi, M.C., Chou, T.T., Bruce, J., Schuck, T., Grossman, M., Clark, C.M., et al. (2006). Ubiquitinated TDP-43 in frontotemporal lobar degeneration and amyotrophic lateral sclerosis. Science *314*, 130–133.

Neumann, M., Mackenzie, I.R., Cairns, N.J., Boyer, P.J., Markesbery, W.R., Smith, C.D., Taylor, J.P., Kretzschmar, H.A., Kimonis, V.E., and Forman, M.S. (2007). TDP-43 in the ubiquitin pathology of frontotemporal dementia with VCP gene mutations. J. Neuropathol. Exp. Neurol. *66*, 152–157.

Nonhoff, U., Ralser, M., Welzel, F., Piccini, I., Balzereit, D., Yaspo, M.L., Lehrach, H., and Krobitsch, S. (2007). Ataxin-2 interacts with the DEAD/H-box RNA helicase DDX6 and interferes with P-bodies and stress granules. Mol. Biol. Cell *18*, 1385–1396.

Ossareh-Nazari, B., Bonizec, M., Cohen, M., Dokudovskaya, S., Delalande, F., Schaeffer, C., Van Dorsselaer, A., and Dargemont, C. (2010). Cdc48 and Ufd3, new partners of the ubiquitin protease Ubp3, are required for ribophagy. EMBO Rep. *11*, 548–554.

Parker, R., and Sheth, U. (2007). P bodies and the control of mRNA translation and degradation. Mol. Cell *25*, 635–646.

Peri, F., and Nüsslein-Volhard, C. (2008). Live imaging of neuronal degradation by microglia reveals a role for v0-ATPase a1 in phagosomal fusion in vivo. Cell *133*, 916–927.

Peters, C., Bayer, M.J., Bühler, S., Andersen, J.S., Mann, M., and Mayer, A. (2001). Trans-complex formation by proteolipid channels in the terminal phase of membrane fusion. Nature *409*, 581–588.

Reijns, M.A., Alexander, R.D., Spiller, M.P., and Beggs, J.D. (2008). A role for Q/N-rich aggregation-prone regions in P-body localization. J. Cell Sci. *121*, 2463–2472.

Salajegheh, M., Pinkus, J.L., Taylor, J.P., Amato, A.A., Nazareno, R., Baloh, R.H., and Greenberg, S.A. (2009). Sarcoplasmic redistribution of nuclear TDP-43 in inclusion body myositis. Muscle Nerve *40*, 19–31.

Sheth, U., and Parker, R. (2003). Decapping and decay of messenger RNA occur in cytoplasmic processing bodies. Science *300*, 805–808.

Sheth, U., and Parker, R. (2006). Targeting of aberrant mRNAs to cytoplasmic processing bodies. Cell *125*, 1095–1109.

Smoot, M.E., Ono, K., Ruscheinski, J., Wang, P.L., and Ideker, T. (2011). Cytoscape 2.8: new features for data integration and network visualization. Bioinformatics *27*, 431–432.

Spriggs, K.A., Bushell, M., and Willis, A.E. (2010). Translational regulation of gene expression during conditions of cell stress. Mol. Cell *40*, 228–237.

Stolz, A., Hilt, W., Buchberger, A., and Wolf, D.H. (2011). Cdc48: a power machine in protein degradation. Trends Biochem. Sci. *36*, 515–523.

Takahara, T., and Maeda, T. (2012). Transient sequestration of TORC1 into stress granules during heat stress. Mol. Cell *47*, 242–252.

Teter, S.A., Eggerton, K.P., Scott, S.V., Kim, J., Fischer, A.M., and Klionsky, D.J. (2001). Degradation of lipid vesicles in the yeast vacuole requires function of Cvt17, a putative lipase. J. Biol. Chem. *276*, 2083–2087.

Wang, C.W., Stromhaug, P.E., Shima, J., and Klionsky, D.J. (2002). The Ccz1-Mon1 protein complex is required for the late step of multiple vacuole delivery pathways. J. Biol. Chem. *277*, 47917–47927.

Wang, X., Fan, H., Ying, Z., Li, B., Wang, H., and Wang, G. (2010). Degradation of TDP-43 and its pathogenic form by autophagy and the ubiquitin-proteasome system. Neurosci. Lett. *469*, 112–116.

Wang, I.F., Guo, B.S., Liu, Y.C., Wu, C.C., Yang, C.H., Tsai, K.J., and Shen, C.K. (2012). Autophagy activators rescue and alleviate pathogenesis of a mouse model with proteinopathies of the TAR DNA-binding protein 43. Proc. Natl. Acad. Sci. USA *109*, 15024–15029.

Wu, Y.T., Tan, H.L., Shui, G., Bauvy, C., Huang, Q., Wenk, M.R., Ong, C.N., Codogno, P., and Shen, H.M. (2010). Dual role of 3-methyladenine in modulation of autophagy via different temporal patterns of inhibition on class I and III phosphoinositide 3-kinase. J. Biol. Chem. *285*, 10850–10861.

Yamamoto, A., Tagawa, Y., Yoshimori, T., Moriyama, Y., Masaki, R., and Tashiro, Y. (1998). Bafilomycin A1 prevents maturation of autophagic vacuoles by inhibiting fusion between autophagosomes and lysosomes in rat hepatoma cell line, H-4-II-E cells. Cell Struct. Funct. *23*, 33–42.

Yorimitsu, T., and Klionsky, D.J. (2005). Autophagy: molecular machinery for self-eating. Cell Death Differ. *12*(*Suppl 2*), 1542–1552.

Zhang, Y., Yan, L., Zhou, Z., Yang, P., Tian, E., Zhang, K., Zhao, Y., Li, Z., Song, B., Han, J., et al. (2009). SEPA-1 mediates the specific recognition and degradation of P granule components by autophagy in C. elegans. Cell *136*, 308–321.

Cell

EXTENDED EXPERIMENTAL PROCEDURES

Transformations and Strain Identification

Strains from the yeast deletion collection (Resgen) were inoculated and grown in 96-well plate format, and subject to a standard Lithium Acetate yeast transformation protocol with plasmid pRP1657. 4249 strains were successfully transformed and subject to microscopic analysis. Conformation of strain identity for all hits in the screen was done via PCR and sequencing of the DNA barcode from the KanMX gene deletion cassette (Winzeler et al., 1999).

Classification of Screen Phenotypes

Screen phenotypes were classified based on the criteria below, relative to multiple averaged measurements from a BY4741 unstressed control:

Strong P body increase $\geq$ 3.5-fold increase in Edc3-mCh average foci number and > 133% average foci size
Moderate P body increase = 3-fold increase in Edc3-mCh average foci number and > average foci size
Weak P body increase $\geq$ 2-fold increase in Edc3-mCh average foci number and > 75% average foci size
Strong P body decrease $\geq$ 4-fold decrease in Edc3-mCh average foci number and < average foci size
Moderate P body decrease $\geq$ 2.5-fold decrease in Edc3-mCh average foci number or > 2-fold decrease in average foci number and < 50% average foci size
Weak P body decrease $\geq$ 2-fold decrease in Edc3-mCh average foci number or > 1.5-fold decrease in average foci number and < 50% average foci size

For comparison, BY4741 exhibit an average of 0.41 foci/cell (±0.20), and an average size of 0.068 μM^2 (±0.015) under nonstress screen conditions.

Strong stress granule increase if > 12% cells exhibit Pab1-GFP foci
Moderate stress granule increase if > 6% cells exhibit Pab1-GFP foci
Weak stress granule increase if > 2% cells exhibit Pab1-GFP foci.

For comparison, BY4741 WT cells exhibit < 0.2% stress granule foci under nonstress screen conditions, thus even weak mutants in our screen exhibit at least a 10-fold increase in cells exhibiting stress granule foci.

Note that strong changes in granule levels can be reflected by different variables (e.g., granule size, intensity, average number/cell, cells exhibiting foci etc). This is why two criteria are used to classify P bodies. Such measures are less practical to enact on large-scale quantitation for stress granules (Buchan et al., 2010); however, the fact that stress granule levels are so close to zero under normal growth conditions gives greater confidence in any mutants in which they are induced.

Quantitation for all strains in final hit list is presented in Table S3.

Yeast Image Analysis

For screen images, semi-automated quantitation of P body number and size was conducted on z stacked data using ImageJ (Schneider et al., 2012) as previously described (Buchan et al., 2010). Owing to signal to noise issues, and high levels of diffuse Pab1-GFP signal, automated quantitation of stress granules was not possible, and thus stress granule foci, and their colocalization or otherwise with P bodies, was recorded on a percentage cell basis. Strains were then assigned into strong, moderate or weak phenotypes based on criteria outlined above and Table S3. Strains exhibiting granule protein mislocalization phenotypes were noted manually (see Table S2).

Percentage of cells exhibiting intravacuolar compartments, as defined by visibly distinct Pab1-GFP structures within vacuoles, was calculated manually, using a minimum of 3 independent replicate experiments and quantitation of at least 200 cells for all strains examined. Cells where vacuoles could not be identified with a high degree of confidence were omitted from such analyses. Colocalization analyses in Figures S6 and S7 were conducted manually, where overlap was defined as two foci exhibiting > 25% total overlap.

All yeast images presented are scaled on equal contrast ranges within experiments using Image J. Single Z slices are shown to aid visualization of organelles and granule colocalization, but quantitation was done on the entire captured z stack (4uM range, 0.25uM slices).

Western Blotting

Mouse monoclonal αGFP (Covance, 1:1000) and goat α mouse horseradish peroxidase (HRP) conjugate (Thermo, 1:2000) were used to detect Pab1-GFP. Mouse monoclonal αPGK1 (Invitrogen) was used to detect endogenous PGK1. Goat α mouse HRP conjugate (Thermo Scientific) was used as a secondary. Standard blotting and visualization procedures were employed. VCP (1:3000; Thermoscientific; MA3-004), and b-actin (1:1000; Sigma-Aldrich; A5316) were visualized by the Odyssey system (Li-Cor). Western blots were quantified using ImageJ software (Schneider et al., 2012).

Transfections/Plasmid Details

HeLa cells were transfected using FuGENE6 transfection reagent (Promega; E2691) following the manufacturer's instructions. The EGFP-VCP wild-type and mutant plasmids were previously described (Tresse et al., 2010).

VCP RNAi knockdown was performed by transfection of ON-TARGET plus-SMARTpool siRNA (Dharmacon; 008727 for human cells) using Lipofectamine RNAi Max (Invitrogen). RNAi knockdown for nontargeting was performed by transfection of ON-TARGET plus-SMARTpool siRNA (Dharmacon; 1081195) using Lipofectamine RNAi Max (Invitrogen).

Real-Time PCR

Total RNA was isolated with Trizol (Invitrogen) from MEFS Atg7wt and Atg7$^{-/-}$. qPCR performed with TaqMan RNA-to Ct 1 step-kit (Applied Biosystems; 4392938). The primers Mm00512209_m1 and 4352339E were used to detect the Atg7 and GAPD, levels, respectively. qPCR was performed in an Applied Biosystems 7900HT Fast Real-Time PCR System using the following cycling parameters: 48°C (15 min), 95°C (10 min), and 40 cycles of 95°C (15 s), 60°C (1 min). All PCR experiments were conducted in triplicate.

HeLa Cell Drug Treatments

Drug additions to HeLa cells included Bafilomycin A1 (0.5 μM; Sigma Aldrich), Sodium Arsenite (1 mM, Sigma Aldrich), Rapamycin (10 nM, Sigma Aldrich), 3-Methyl adenine ('3-MA'; 10 μM, Sigma), Wortmannin (1.5 μM, Sigma), Sorbitol (0.6 M, Sigma), Clotrimazole in DMEM serum free media (20 μM, Sigma), DBeQ (10 μM, Sigma), ML240 (2.5 μM, gift from Dr TF Chou) and EerI (8 μM, Sigma).

HeLa and MEF Immunofluorescence Antibodies

HeLa cells were stained for stress granules with the following primary antibodies: HuR mouse monoclonal IgG (1:200 dilution; Abcam), eIF3η goat (1:200; Santa Cruz Biotechnology, Inc.), TIAR mouse monoclonal (1:200; BD Transduction Laboratories), G3BP mouse monoclonal (1:350; BD Transduction Laboratories), and eIF4G rabbit polyclonal (1:200; Santa Cruz). Goat α-mouse Texas red (1:400; Santa Cruz Biotechnology, Inc.), donkey α-mouse Alexa 488 and 647, donkey α-goat Alexa 488 and 555, donkey α-rabbit Alexa 555 and 647 (1:400; Invitrogen) were used as secondary antibodies. MEFs were stained for eIF3η, TIAR and HuR as above. RCK rabbit polyclonal IgG (1:250; MBL International) and donkey α-rabbit Alexa 488 (1:400; Invitrogen) were used for P body staining. VCP and TDP-43 staining utilized VCP mouse monoclonal antibody IgG (1:50; BD Transduction Laboratories) and TDP-43 rabbit polyclonal antibodies (1:350; Proteintech).

Statistical Analysis

Statistical analysis of IVC clearance, stress granule clearance and protein quantitation were evaluated by the paired Student's t test at $p < 0.05$ with Excel (Microsoft).

SUPPLEMENTAL REFERENCES

Buchan, J.R., Nissan, T., and Parker, R. (2010). Analyzing P-bodies and stress granules in Saccharomyces cerevisiae. Methods Enzymol. *470*, 619–640.

Coller, J., and Parker, R. (2005). General translational repression by activators of mRNA decapping. Cell *122*, 875–886.

Dunckley, T., and Parker, R. (2001). Yeast mRNA decapping enzyme. Methods Enzymol. *342*, 226–233.

Hatfield, L., Beelman, C.A., Stevens, A., and Parker, R. (1996). Mutations in trans-acting factors affecting mRNA decapping in Saccharomyces cerevisiae. Mol. Cell. Biol. *16*, 5830–5838.

Hsieh, M.T., and Chen, R.H. (2011). Cdc48 and cofactors Npl4-Ufd1 are important for G1 progression during heat stress by maintaining cell wall integrity in Saccharomyces cerevisiae. PLoS ONE *6*, e18988.

Huh, W.K., Falvo, J.V., Gerke, L.C., Carroll, A.S., Howson, R.W., Weissman, J.S., and O'Shea, E.K. (2003). Global analysis of protein localization in budding yeast. Nature *425*, 686–691.

Shintani, T., Huang, W.P., Stromhaug, P.E., and Klionsky, D.J. (2002). Mechanism of cargo selection in the cytoplasm to vacuole targeting pathway. Dev. Cell *3*, 825–837.

Schneider, C.A., Rasband, W.S., and Eliceiri, K.W. (2012). NIH Image to ImageJ: 25 years of image analysis. Nat. Methods *9*, 671–675.

Swisher, K.D., and Parker, R. (2010). Localization to, and effects of Pbp1, Pbp4, Lsm12, Dhh1, and Pab1 on stress granules in Saccharomyces cerevisiae. PLoS ONE *5*, e10006.

Tresse, E., Salomons, F.A., Vesa, J., Bott, L.C., Kimonis, V., Yao, T.P., Dantuma, N.P., and Taylor, J.P. (2010). VCP/p97 is essential for maturation of ubiquitin-containing autophagosomes and this function is impaired by mutations that cause IBMPFD. Autophagy *6*, 217–227.

Winzeler, E.A., Shoemaker, D.D., Astromoff, A., Liang, H., Anderson, K., Andre, B., Bangham, R., Benito, R., Boeke, J.D., Bussey, H., et al. (1999). Functional characterization of the S. cerevisiae genome by gene deletion and parallel analysis. Science *285*, 901–906.

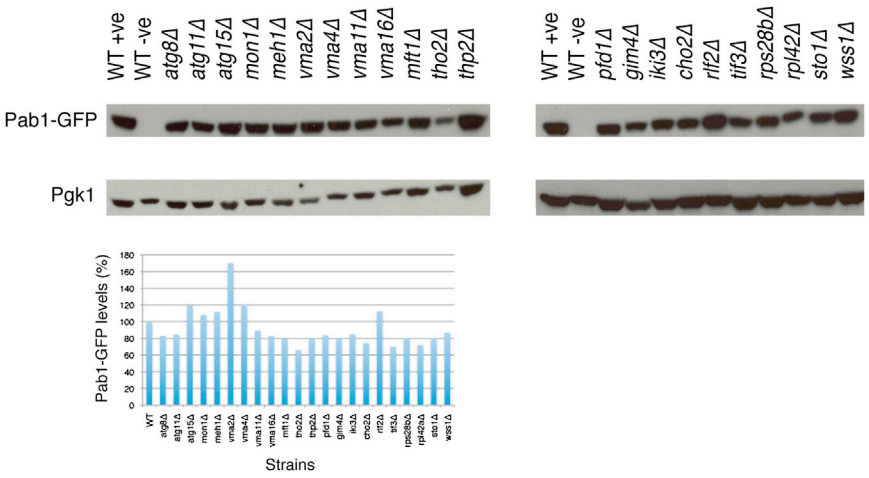

Figure S1. Expression Levels of Granule Marker Proteins Vary Only Modestly in a Subset of Screen Hits, Related to Figure 1

Pab1-GFP levels expressed via pRP1657 were determined in the listed strains relative to endogenous PGK1 levels under nonstress logarithmic growth conditions.

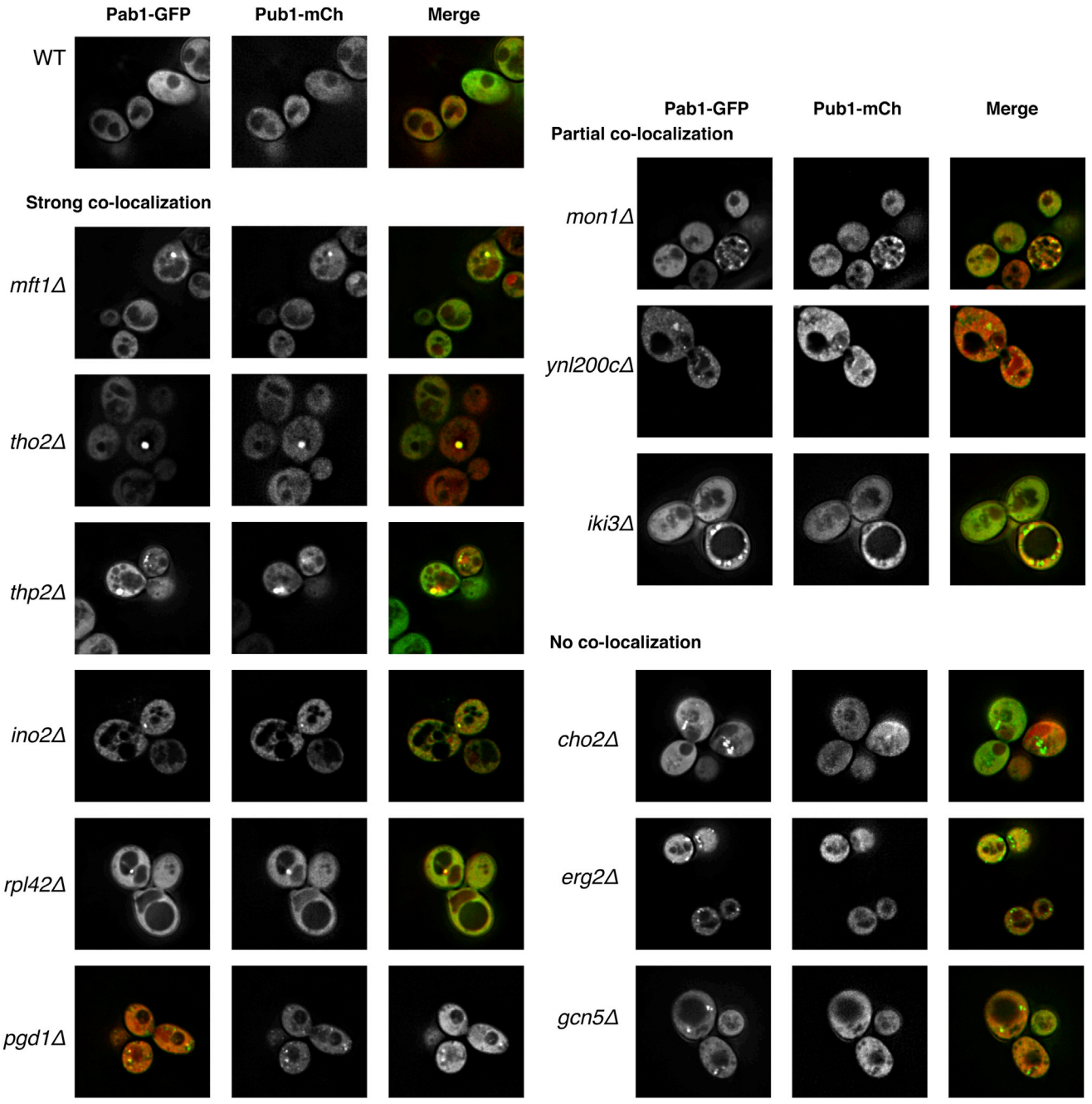

Figure S2. Screen Hits Exhibit Pab1-GFP Foci that Typically Colocalize with Pub1-mCh, Related to Figure 1

Strains were transformed with pRP1363 (Pab1-GFP) and pRP2150 (Pub1-mCh) and examined in the indicated null-strain backgrounds under logarithmic growth.

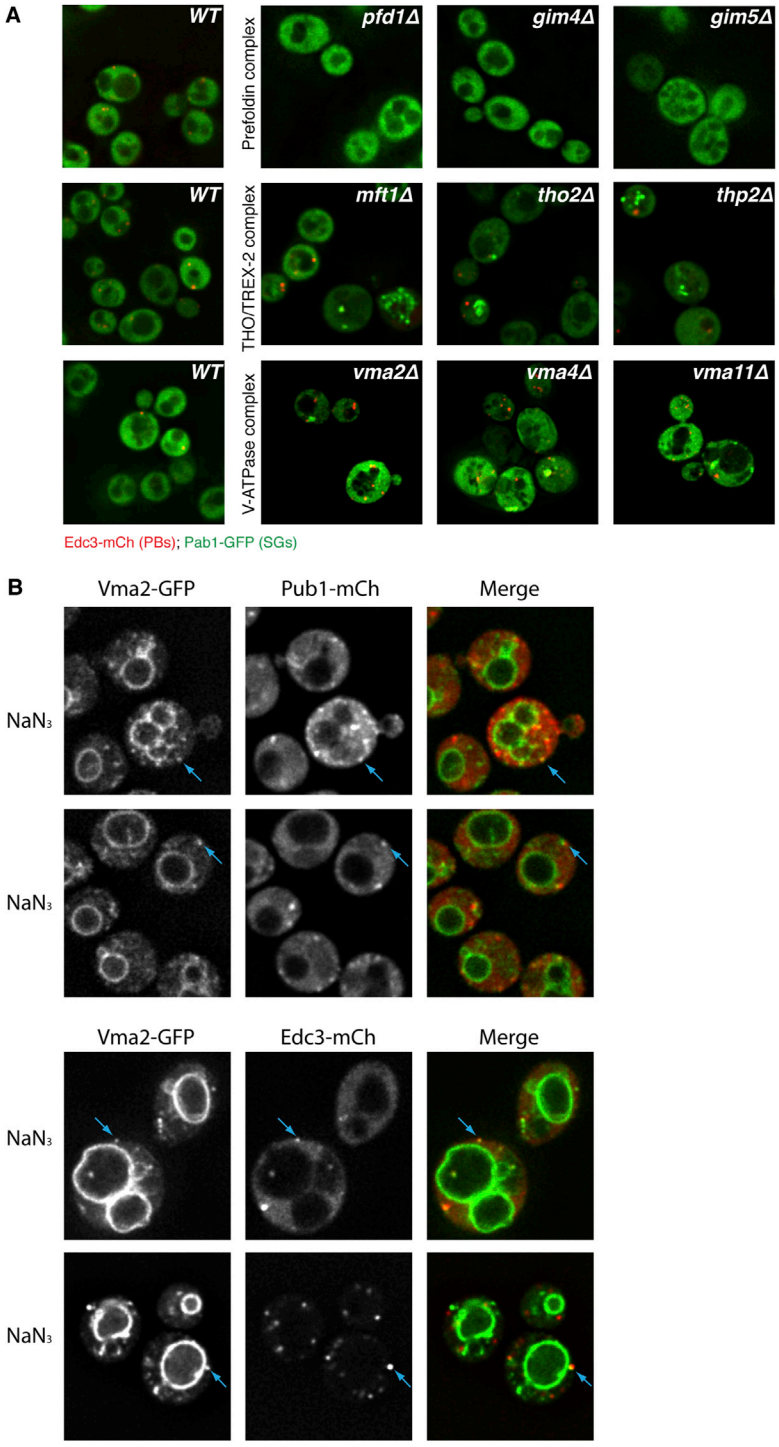

Figure S3. Multiple Screen Hits Map to Various Molecular Complexes with Similar Phenotypes and Include Novel Granule Components, Related to Figure 1

(A) Pab1-GFP and Edc3-mCh serve as stress granule and P body markers respectively. WT cells exhibit modest P bodies, whereas prefoldin complex deletions exhibit decreased P bodies, THO/TREX-2 complex deletions exhibit P body distinct stress granules and mislocalized signal (e.g., nuclear Pab1-GFP), and Vacuolar ATPase gene deletions exhibit stress granules that colocalize with some P bodies.

(B) Vma2-GFP strains, transformed with pRP1661 (Pub1-mCh) or pRP1574 (Edc3-mCh), were subject to 0.5% v/v NaN_3 stress for 20 min in midlog. Blue arrows indicate examples of colocalization.

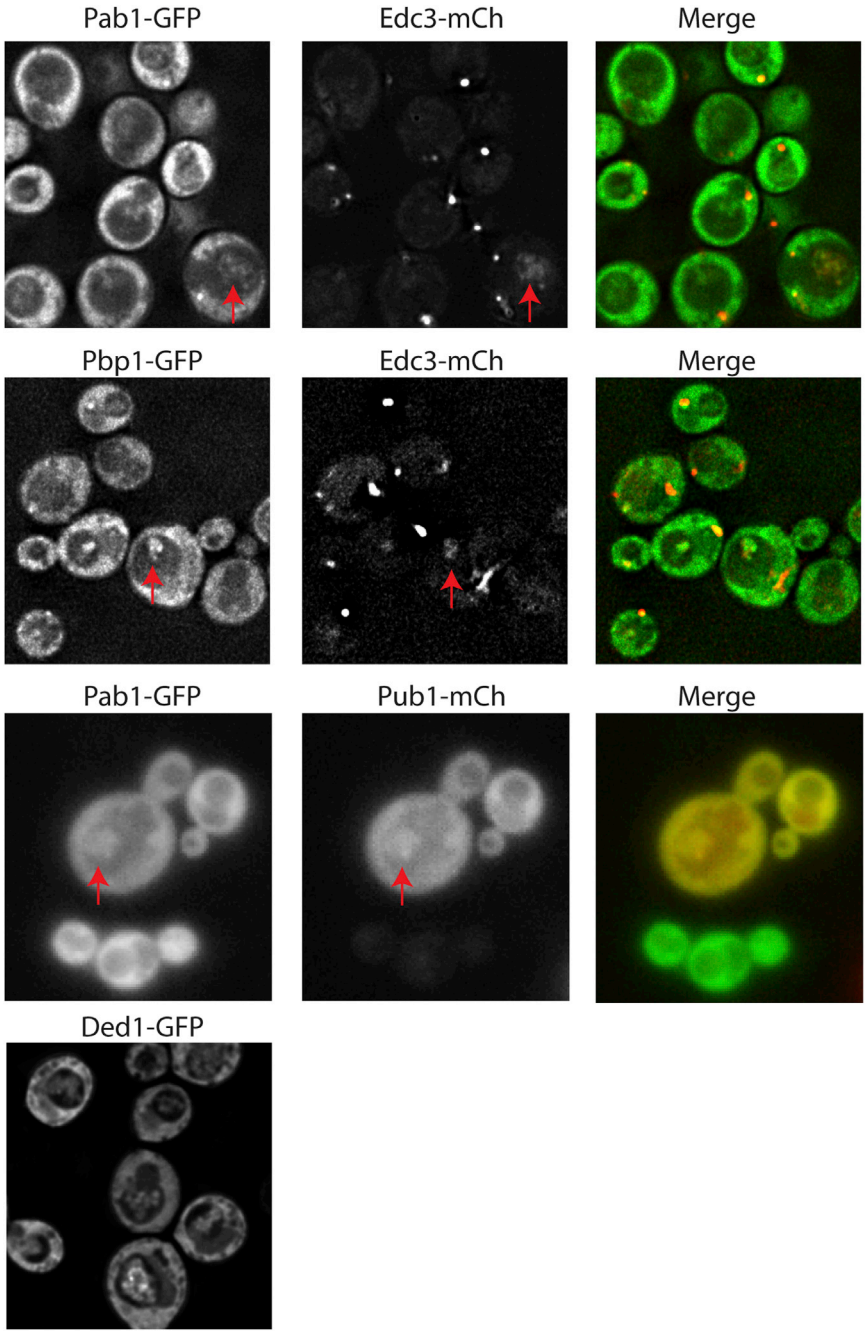

Figure S4. Composition of Intravacuolar Compartment in *atg15Δ*, Related to Figure 2

RP840 *atg15Δ* strain transformed with pRP1657 (Pab1-GFP, Edc3-mCh), pRP1944- (Pbp1-GFP, Edc3-mCh), pRP1362 (Pab1-GFP) and pRP1661 (Pub1-mCh) in combination, or pRP1556 (Ded1-GFP). Red arrows highlight colocalization; note that Edc3 signal is typically weaker than that of Pab1-GFP, and not always visible in Pab1-containing intravacuolar compartments.

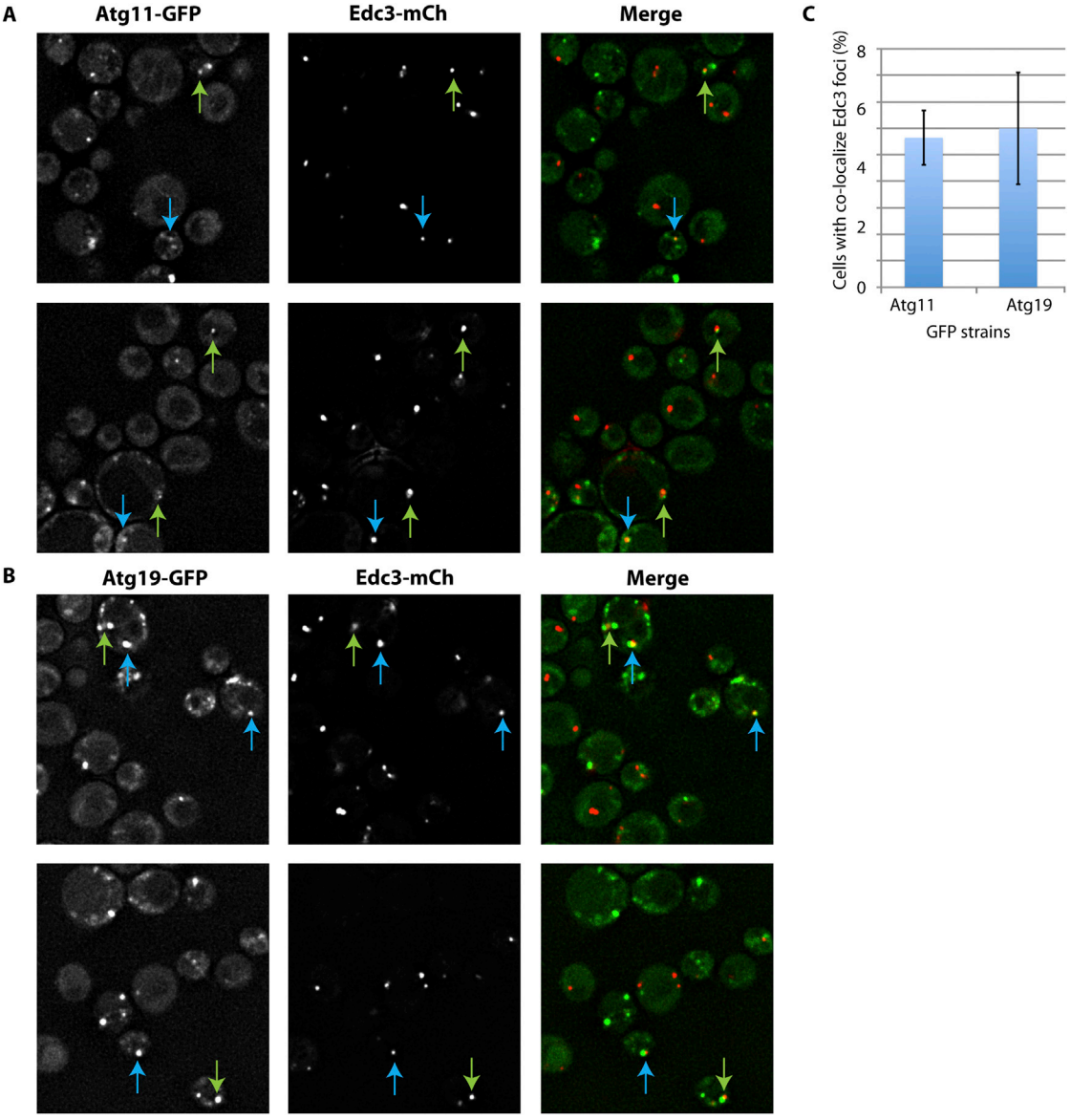

Figure S5. Edc3-Foci Exhibit Low-Level Colocalization with Autophagy Machinery Components, Related to Figure 2

(A) BY4741 chromosomal Atg11-GFP strain, transformed with pRP1574 (Edc3-mCh) and examined in early stationary phase. Blue arrows indicate complete overlap of foci; green arrows a partial overlap (see Experimental Procedures).

(B) BY4741 chromosomal Atg19-GFP strain, details as in (A).

(C) Quantitation of overlap in (A) and (B), mean values ± data range based on two replicate experiments.

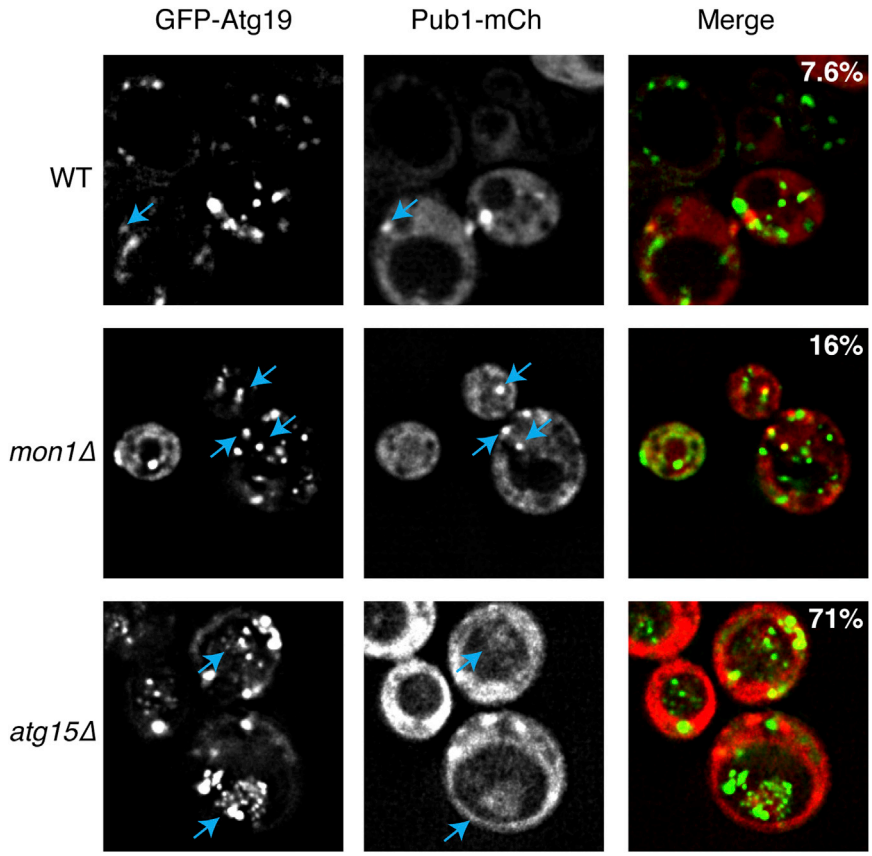

Figure S6. Pub1 Colocalizes with Atg19 in Distinct Cellular Compartments Depending on Blocks in Autophagy, Related to Figure 2
BY4741 strains expressing pRP1661 (Pub1-mCh) and GFP-Atg19 (pRP2447) were examined in early stationary phase. Arrows indicate areas of overlap, with numbers in image indicating percentage of cells exhibiting colocalizing foci (WT, *mon1Δ*) or Pub1-mCh IVCs exhibiting partial/complete overlap with GFP-Atg19 *(atg15Δ)*.

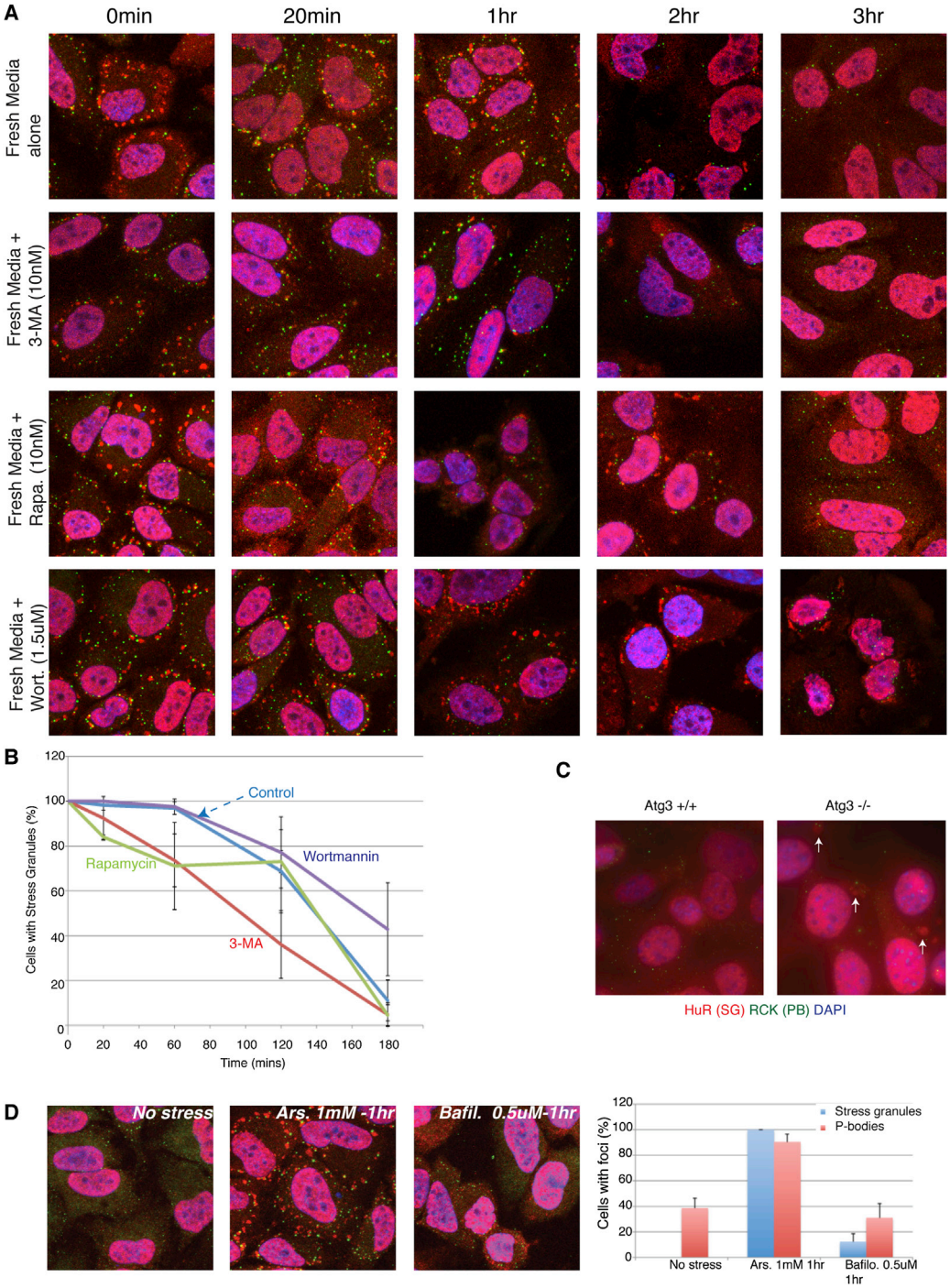

Figure S7. Chemical and Genetic Perturbation of Autophagy Affects Stress Granule Clearance, Related to Figure 5

(A) Immunofluorescence of HeLa cells stained with DAPI (blue, nucleus), RCK (green, P bodies) and HuR (red, stress granules). Cells were treated with 1 mM arsenite for 1 hr, followed by recovery in fresh media ±10 μM 3-MA (Autophagy enhancer), 10 nM Rapamycin (Autophagy enhancer) or 1.5 μM Wortmannin (Autophagy inhibitor).

(B) Quantitation of (A), mean values base on a minimum of three replicate experiments ± SD.

(C) Immunofluorescence of Atg3$^{-/-}$ MEF lines following inoculation at 25% confluency and growth for 2.5 days. Cells stained with DAPI (blue, nucleus), RCK (green, P bodies) and HuR (red, stress granules). Arrows indicate stress granules.

(D) Immunofluorescence of HeLa cells treated with media alone (−ve control) 1 mM Arsenite (+ve control), or 0.5 μM Bafilomycin (V-ATPase inhibitor). Cells stained with DAPI (blue, nucleus), RCK (green, P bodies) and HuR (red, stress granules). Quantitation consists of mean values ± SD based on a minimum of three replicate experiments.